THE DIRECTIONAL STABILITY AND CONTROL OF AN AIRPLANE DURING THE LANDING ROLL

by

Andrew J. Gorechlad

Thesis submitted to the Graduate Faculty of the

Virginia Polytechnic Institute

in candidacy for the degree of

MASTER OF SCIENCE

in

AEROSPACE ENGINEERING

APPROVED:

Chairman, Dr. James B. Eades, Jr.

April 1967

Blacksburg, Virginia

TABLE OF CONTENTS

I. LIST OF FIGURES

II. SUMMARY

An analysis of airplane dynamics during the ground roll after landing is presented. This analysis was performed for an airplane having the size and characteristics of a high-speed fighter-bomber. However, the results obtained here are sufficiently general in nature to be applicable to most aircraft. Actually, the results are typical of aircraft with tricycle landing gear.

The non-linear equations of motion developed in this thesis were solved on an Applied Dynamics analog computer. Several assumptions, including constant friction coefficients and tire operation at rated conditions, were made to reduce the equations to a form suitable for the computer.

For this study, the parameters used in the equations of motion are only approximate quantities. This is especially true of the tire and wheel properties since these are difficult to predict and can be obtained only by testing a given tire over a given surface. Factors such as the influence of tire wear, the effect of temperature, and the seasonal variations of runway surfaces make the task of determining exact values for tire and wheel properties impossible.

III. INTRODUCTION

An airplane in the process of decelerating, while rolling down the runway after the landing touchdown, may encounter environmental disturbances such as wind gusts which will affect its directional motion. In recent years there have been several instances where aircraft have skidded off the runway while landing or taxying. According to reference 1, in the United States during the years 1956-1961, there were 23 cases of airplanes veering off the runway as compared with 21 cases of overshoot. Some of these accidents occurred under adverse weather conditions, i.e., water-covered or frozen runways, but a number of incidents occurred on dry runways under good operating conditions.

This study was conducted to determine the causes of directional instability during the landing roll, and to suggest possible remedies for the problem. It is of fundamental interest to investigate the tendency of an airplane equipped with tricycle landing gear to sideslip while rolling on a runway and to examine its ability to recover from a skidding situation.

The influence of landing gear placement and arrangement upon the lateral stability of the airplane was considered. Essentially, this consisted of studying the effect of varying the distance between the nose gear and the main gear, the spacing between the main gear, tire

size and pressure, and the effect of the vertical loading upon tire characteristics. The principle area of investigation was that of a freely rolling aircraft on a dry runway; however, braked rolling and wet and icy runways were also considered.

In addition to the above considerations, aerodynamic effects were investigated even though the landing ground roll takes place at relatively low speeds. The effects of lift and pitching moment upon wheel loadings and the contribution of aerodynamic directional stability were examined.

A limited control analysis was performed to ascertain whether or not skidding could be overcome through the application of a suitable control force. The analysis was restricted to a study of directional response, of the airplane, to the application of either rudder aerodynamics or nosewheel steering. Since the nosewheel is often locked at high rolling speeds, in the interest of preventing nosewheel shimmy, the rudder is the principle form of directional control. However, when the airplane has slowed to the point where nosewheel shimmy is no longer a problem, and where the aerodynamic control lacks sufficient power, the nosewheel becomes the primary form of directional control. Differential braking and banking of the airplane during the ground roll were considered as alternate forms of control; but, since these were more difficult to simulate, they were not included in the analysis. Also, the influence of the longitudinal control, i.e.,

elevator or horizontal stabilizer, upon the wheel loadings was investigated.

IV. LIST OF SYMBOLS

A	tire footprint area, in^2
C_L	lift coefficient
C_D	drag coefficient
C_ℓ	rolling moment coefficient
C_{ℓ_r}	rotary or cross derivative, $\frac{\partial C_\ell}{\partial r}$, per rad/sec
C_{ℓ_β}	dihedral effect, $\frac{\partial C_\ell}{\partial \beta}$, per radian
$C_{\ell_{\delta_a}}$	aileron control power, $\frac{\partial C_\ell}{\partial \delta_a}$, per radian
C_m	pitching moment coefficient
C_{m_α}	longitudinal static stability derivative, $\frac{\partial C_m}{\partial \alpha}$, per radian
$C_{m_{\delta_e}}$	elevator control power, $\frac{\partial C_m}{\partial \delta_e}$, per radian
$C_{m_{\delta_{hs}}}$	horizontal stabilizer control power, $\frac{\partial C_m}{\partial \delta_{hs}}$, per radian
C_n	yawing moment coefficient
C_{n_r}	yaw damping derivative, $\frac{\partial C_n}{\partial r}$, per rad/sec
C_{n_β}	directional static stability derivative, $\frac{\partial C_n}{\partial \beta}$, per radian
$C_{n_{\delta_r}}$	rudder control power, $\frac{\partial C_n}{\partial \delta_r}$, per radian
C_y	side force coefficient
C_{y_β}	side force derivative, $\frac{\partial C_y}{\partial \beta}$, per radian
D	drag force, lbs

F	force, lbs
F_{r_x}	frictional drag force, lbs
F_{r_y}	frictional side or cornering force, lbs.
H	angular momentum, ft-lbs-sec^3
I_N	moment of inertia of the nosewheel about the steering axis, slug-ft^2
I_x, I_y, I_z	moments of inertia about the x-, y-, and z-axes, respectively, slug-ft^2
I_{xy},I_{yz},I_{zx}	products of inertia, slug-ft^2
K	tire cornering power, lbs/radian (defined as N in reference 2)
L	lift force, lbs
L	aerodynamic rolling moment or a moment about the x-axis, ft-lbs
M	aerodynamic pitching moment or a moment about the y-axis, ft-lbs
N	aerodynamic yawing moment or a moment about the z-axis, ft-lbs
R	ground reaction resultant acting on the landing gear wheels, lbs
S	wing area, ft^2
T	thrust, lbs
T_z	tire self-aligning torque, in-lbs
T_b	braking torque, ft-lbs
V	velocity, ft/sec
V_c	velocity of the point of contact of a rolling wheel, ft/sec

V_h	minimum hydroplaning velocity, ft/sec
W	weight, lbs
Y	aerodynamic side force, lbs
a	acceleration, ft/sec^2
b	wing span, ft
d	tire or wheel diameter, inches
$\vec{e}_x$, $\vec{e}_y$, $\vec{e}_z$	units vectors along the x-, y-, and z-axes, respectively
g	acceleration of gravity, 32.17 ft/sec^2
h	angular momentum, $ft\text{-}lb\text{-}sec^3$
k	effective distance between nosewheel and mainwheels defined by Eq. (56)
m	mass, slugs
p, q, r	angular velocities about the x-, y-, and z-axes, respectively
p	tire inflation pressure, lbs/in^2
q	pneumatic castor, inches
r_w	tire radius of an unloaded wheel, inches
s_l	slip ratio
u, v, w	translational velocities in the x-, y-, and z-directions, respectively, ft/sec
w	tire or wheel width, inches
x_c	location of the ground pressure resultant R from a point beneath the axle, inches
x_M	distance from the center of gravity to the main landing gear axle along the x-axis, ft

x_N	distance from the center of gravity to the nosewheel axle along the x-axis, ft
y_M	distance from the center of gravity to the center of the main landing gear wheel along the y-axis, ft
z_G	distance from the center of gravity to the runway surface along the z-axis
α	angular acceleration, rad/sec^2
α_L	angle of attack during the ground roll, radians
β	angle of sideslip or skid, radians
δ_a	aileron deflection, radians
δ_e	elevator deflection, radians
δ_{hs}	deflected angle of the horizontal stabilizer, radians
δ_r	rudder deflection, radians
δ_w	vertical tire or wheel deflection, inches
λ	a dimensionless parameter defined by Eq. (B-4)
λ'	a dimensionless parameter defined by Eq. (B-6)
μ_{av}	coefficient of average braking friction
μ_b	coefficient of braking friction
μ_{max}	coefficient of maximum braking friction
μ_r	coefficient of rolling friction
μ_s	coefficient of skidding friction
μ_x	coefficient of friction in the x-direction
μ_y	coefficient of side friction
ω	angular velocity, rad/sec

ρ	atmospheric density, slugs/ft^3
σ	the dimensionless ratio, μ_s/μ_{max}
ψ	yaw or heading angle, radians
$\dot{\psi}$	angular velocity about a direction perpendicular to the runway, rad/sec
θ	a dimensionless parameter defined by Eq. (B-3)
θ'	a dimensionless parameter defined by Eq. (B-5)
ξ	effective skidding angle of a swiveling nosewheel

Subscripts

o	initial conditions
M	main landing gear wheels
LM	left main landing gear wheel or wheels
RM	right main landing gear wheel or wheels
N	nosewheel
rat	rated tire conditions
x, y, z	components along the x-, y-, and z-axes, respectively

Notation

$(\dot{\ })$	derivative with respect to time, $\frac{d}{dt}(\ )$
$\vec{(\ )}$	vector quantity
$\lvert(\ )\rvert$	absolute value

V. ANALYSIS

(A) General Equations of Motion.

From Appendix A, the general equations of motion with respect to a set of body axes for an airplane are:

$$\sum F_x = m(\dot{u} + wq - vr)$$
$$\sum F_y = m(\dot{v} + ur - wp)$$
$$\sum F_z = m(\dot{w} + vp - uq)$$

$$\sum L = I_x\dot{p} - I_{xz}\dot{r} + (I_z - I_y)\, qr - I_{xz}\, pq$$
$$\sum M = I_y\dot{q} + (I_x - I_z)\, rp + I_{xz}\,(p^2 - r^2)$$
$$\sum N = I_z\dot{r} - I_{xz}\dot{p} + (I_y - I_x)\, pq + I_{xz}\, qr$$

However, for an airplane moving down a runway during ground roll, the following constraints are applied to the general equations:

i) no translation in the z-directions: $w = o$, $\dot{w} = o$

ii) no rotation about the roll axis: $p = o$, $\dot{p} = o$

iii) no rotation about the pitch axis: $q = o$, $\dot{q} = o$

Thus the equations of motion reduce to:

$$\sum F_x = m(\dot{u} - vr) \qquad (1)$$
$$\sum F_y = m(\dot{v} + ur) \qquad (2)$$
$$\sum F_z = 0 \qquad (3)$$

$$\sum L = - I_{xz} \dot{r} \tag{4}$$

$$\sum M = - I_{xz} r^2 \tag{5}$$

$$\sum N = I_z \dot{r} \tag{6}$$

Next, an evaluation of the left-hand sides of the equations of motion requires an examination of the forces and moments acting on the airplane. These forces and moments may be separated into the following groups:

1. Wheel and landing gear forces
2. Aerodynamic forces
3. Aerodynamic moments
4. Gravity forces
5. Thrust

Since the equations of motion are written relative to a set of body axes it is necessary to consider the forces relative to these axes.

(B) Wheel and Landing Gear Forces.

With the intention of simplifying the discussion of wheel and landing gear forces, a freely rolling, unbraked wheel will be considered first. Then the discussion will be expanded to include an examination of a wheel subject to braked rolling. The discussion will be concerned mainly with dry runway surfaces, but wet and icy surfaces will be inspected briefly.

The forces and moments acting on an unbraked, yawed[1] wheel are shown in Figure 1.

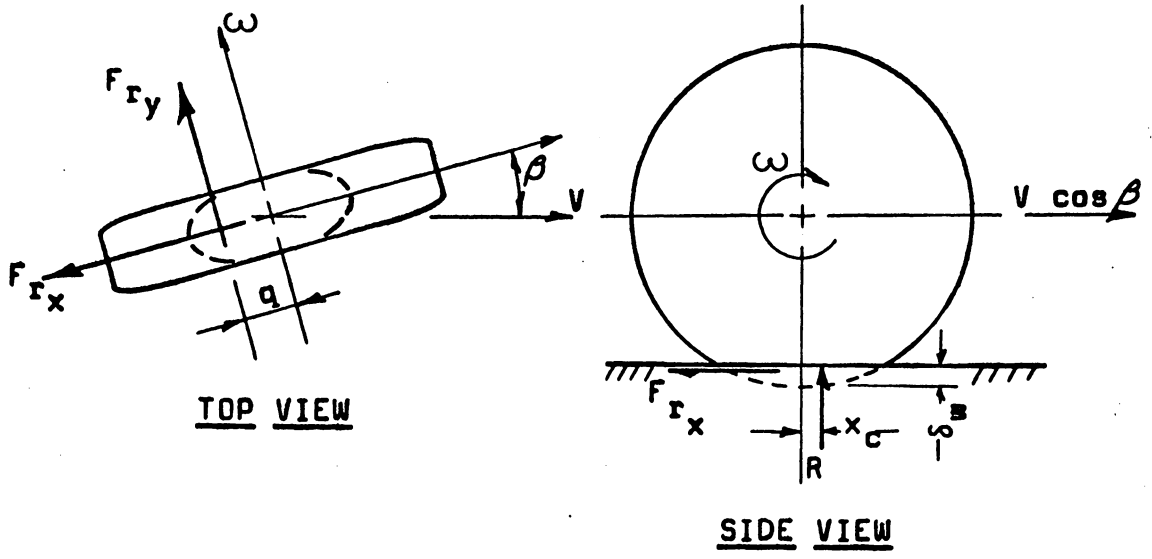

Figure 1. Forces acting on a yawed wheel

The ground reaction force, R, is the resultant of the pressure distribution due to the runway surface, which is supporting the tire. The profile of this pressure distribution is shown in Figure 2 for an unyawed ($\beta = 0$) wheel rolling at a constant speed. The location of the ground reaction force, R, is defined as the center of ground

---

1) Note that when referring to tire or wheel properties, the term yaw is often interchanged with the terms sideslip and skid and the symbols ψ and β are used synonymously. This situation exists because tire and wheel tests are conducted in a straight line, giving rise to the condition $\beta = -\psi$.

pressure, x_c. However, since x_c is much smaller than the distances between the landing gear, it will be assumed that x_c is zero and that the ground reaction resultant acts directly under the axle of the wheel.

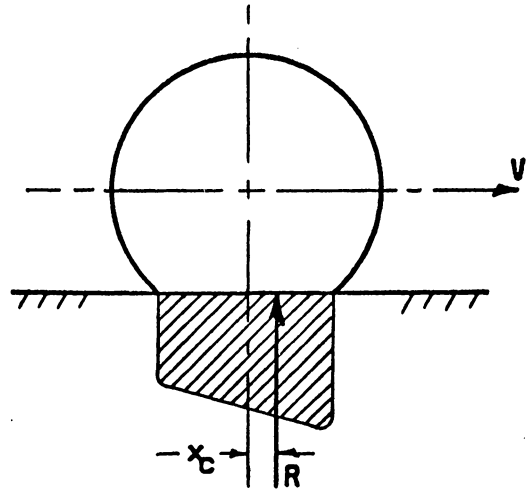

Figure 2. Vertical load distribution on the footprint of a rolling tire

The force, F_{r_x}, in the plane of the wheel is defined as the frictional drag force of the tire. It is this frictional resistance which overcomes the internal frictional losses about the wheel's axle and maintains the angular velocity of the wheel under a condition of zero slip. The rolling resistance is given by the relation

$$F_{r_x} = \mu_r R \tag{7}$$

where μ_r is the coefficient of rolling friction and is a function of tire size, pressure, loading, velocity, and the angle of sideslip, β. A complete discussion of the coefficient of rolling friction is presented in Appendix B.

Values of μ_r are given by the empirical equation (B-7) in Appendix B. However, this relation is very bulky and a simplification

of equation (B-7) is necessary. Therefore, it will be assumed that the curve given by Equation (B-7) may be replaced with an average constant value of θ' defined as

$$\theta' = \text{constant}$$

This approximation is depicted in Figure 3.

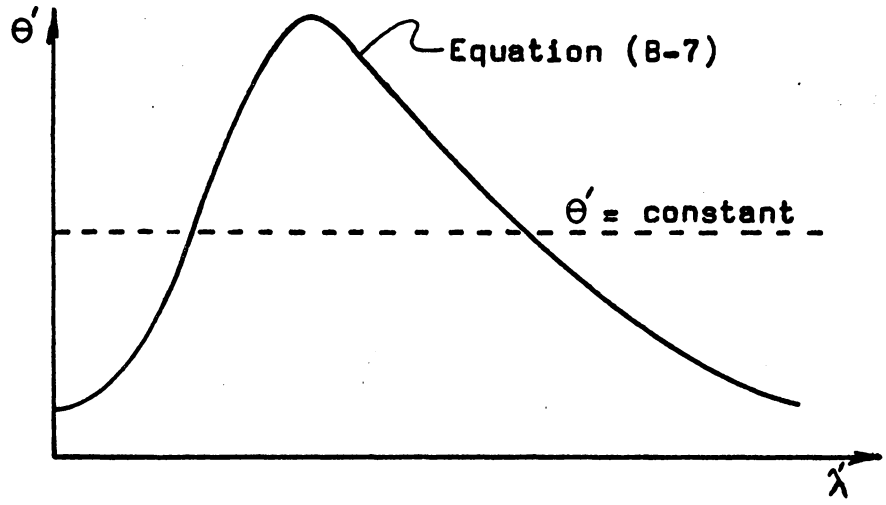

Figure 3. Coefficient of rolling friction approximation

Thus, it will be assumed that

$$\theta' = \frac{400\ p\ R_{rat}}{p_{rat}\ R\ (V + 400)} \left(\frac{d}{w} \right)^2 \mu_r = 0.12 \qquad (8)$$

where V is in feet per second. Now, if it is assumed that the tire is operating at or near rated conditions, then

$$\frac{p\, R_{rat}}{p_{rat}\, R} \approx 1$$

and Eq. (8) is further reduced to

$$\mu_r = 0.12 \left(\frac{W}{d} \right)^2 \left(1 + \frac{V}{400} \right) . \qquad (9)$$

However, since it is desirable to have μ_r independent of V when solving the equations of motion, then an average value of V will be used in Eq. (9). Thus, it will be assumed that μ_r is constant during the landing roll.

The force, F_{r_y}, acting perpendicular to the plane of the tire is defined as the tire cornering force. The cornering force acts only when the tire is moving at an angle β with respect to its forward velocity as shown in Figure 1; F_{r_y} is zero when $\beta = 0$. Since the cornering force, F_{r_y}, acts behind the center of the tire footprint, it tends to return the tire to the unyawed position, thus giving rise to a self-aligning torque, T_z, according to the relation

$$T_z = F_{r_y}\, q \qquad (10)$$

where q is defined as the pneumatic castor. However, when considering the side force in the equations of motion, the pneumatic castor, q, will be neglected since

$$q \ll x_M + x_N \; ; \quad q \ll y_M \; .$$

Thus, it will be assumed that $T_z = 0$.

The variation of the cornering force with the angle of sideslip β is shown in Figure 4. In this figure the dimensionless ratios $\frac{F_{r_y}}{\mu_y R}$ and $\frac{K}{\mu_y R}\beta$ are plotted against each other.

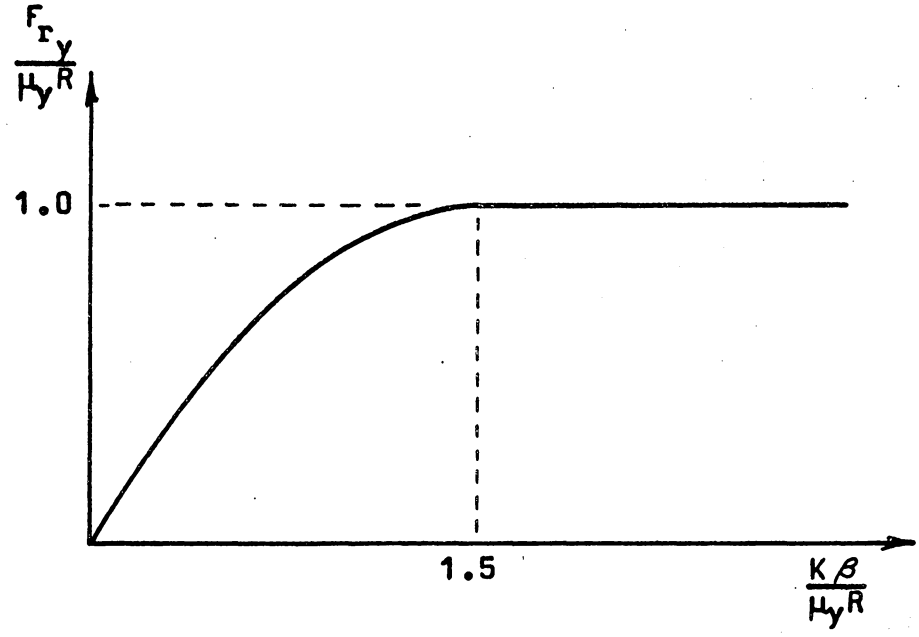

Figure 4. Empirical relation for the cornering force

According to reference 2, the empirical relationships describing the curve in Figure 4 are

$$\frac{F_{r_y}}{\mu_y R} = \frac{K\beta}{\mu_y R} - \frac{4}{27}\left(\frac{K\beta}{\mu_y R}\right)^3 \quad \text{for} \quad \left|\frac{K\beta}{\mu_y R}\right| \leq 1.5$$

and (11)

$$\frac{F_{r_y}}{\mu_y R} = 1 \quad \text{for} \quad \left|\frac{K\beta}{\mu_y R}\right| \geq 1.5$$

where μ_y is the coefficient of side friction and K is the tire cornering

power. Note that F_{r_y} varies linearly for small values of β; and for large values it approaches the asymptotic value, $\mu_y R$.

The coefficient of side friction, μ_y, is a function of tire pressure, aircraft velocity, and runway surface conditions. However, there are no relationships available which will give the value of μ_y for a given set of conditions. But, this situation can be circumvented if it is assumed that

$$\mu_y = \mu_s ,$$

where μ_s is the coefficient of skidding friction. Reference 3 states that the coefficient of side friction is equivalent to the coefficient of skidding friction, or that "μ_y and μ_s are substantially the same. Some examples of the difference between them are shown . . . . ., but in view of the difficulty of accurate measurement, the assumption seems reasonable."

Therefore, since there is an abundant quantity of empirical data for the coefficient of skidding friction, the above assumption can be used advantageously to obtain values for the coefficient of side friction. A summary of existing data giving the value of μ_s on dry concrete is presented in Figure 5, and by Eqs. (12) and (13). Values of μ_s for dry bituminous surfaces are, in general, slightly lower, but for all practical purposes can be considered to be the same.

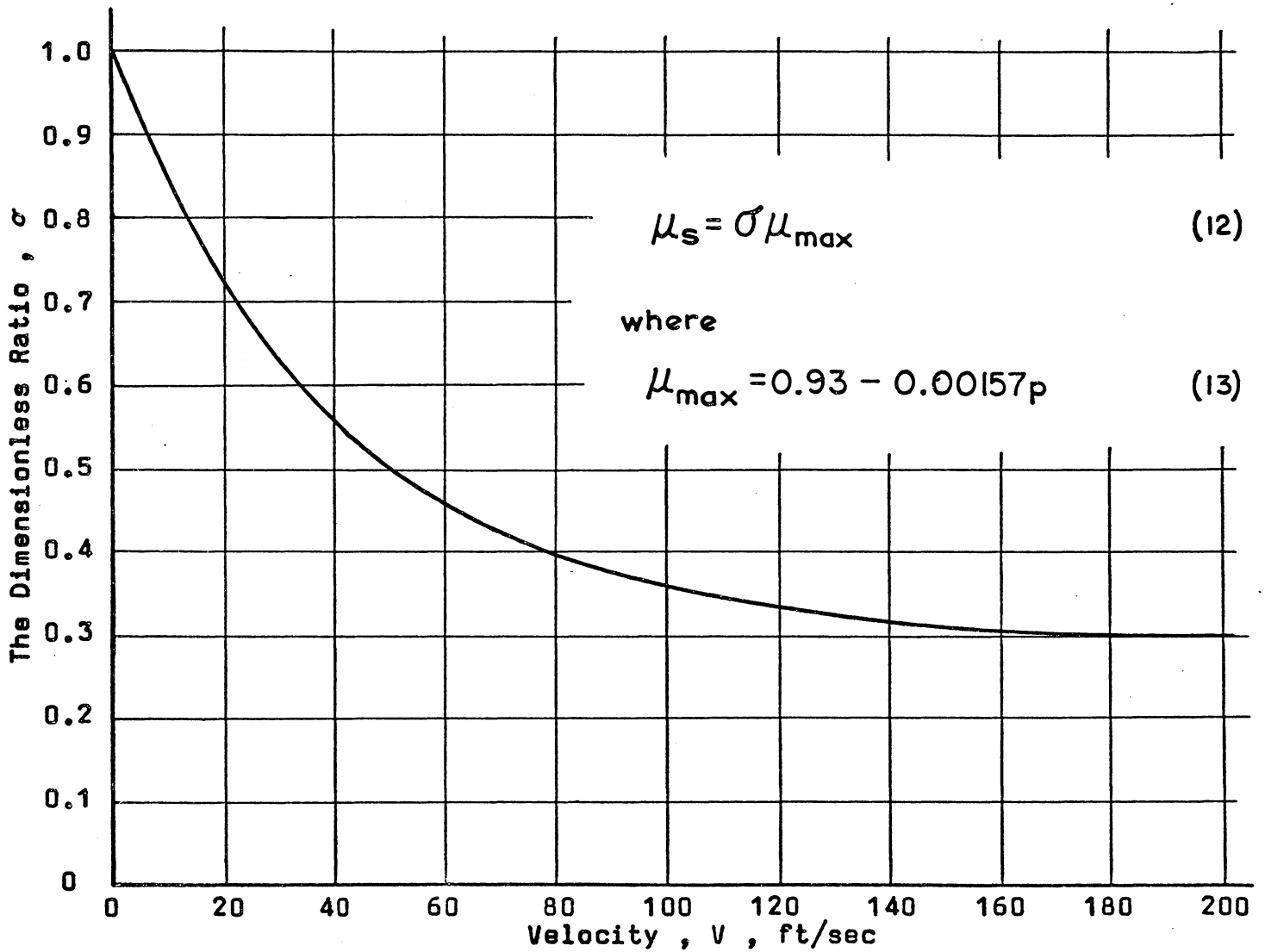

Figure 5. The ratio μ_s/μ_{max} as a function of velocity on dry concrete surfaces

It will be noted from Figure 5 that μ_y will vary during the landing roll; but, as with the coefficient of rolling friction, it will be assumed that μ_y is a constant. An average value of the coefficient of side friction will be used in the equations of motion.

The cornering power, K, is defined as the rate of change of the cornering force, F_{r_y}, with yaw angle, β, for $\beta = 0$; or

$$K = \left.\frac{dF_{r_y}}{d\beta}\right|_{\beta=0} . \tag{14}$$

The cornering power is a function of tire pressure and the vertical deflection, δ_w, of the wheel. Thus, since δ_w is influenced by the vertical load on the wheel, which in turn is affected by the aerodynamic lift acting on the airplane, it can be seen that the cornering power, K, will vary during the landing roll.

It would be very convenient if K would be a constant since this would simplify the equations of motion greatly. Therefore, it will be assumed that the tire is always operating at rated conditions; this will allow K to be considered as a constant.

For the rated vertical deflection, the cornering power, K, can be obtained from the empirical relation

$$\frac{K}{57(p + 0.44\ p_{rat})\ w^2} = 0.038 \tag{15}$$

or, since the tire is operating at rated conditions, $p = p_{rat}$, and Eq. (15) can be rewritten as

$$K_{rat} = 3.12\ p_{rat}\ w^2 \quad . \tag{16}$$

Here K has the units of pounds per radian.

Similarly, at the rated vertical deflection the ground reaction, R, is given by the empirical equation

$$R_{rat} = 0.08\ p_{rat}\ d^2 \quad . \tag{17}$$

By combining Eqs. (16) and (17) an approximate relation for the ratio, $\frac{K}{R}$, is obtained; thus

$$\frac{K}{R} = \frac{K_{rat}}{R_{rat}} = 39\ \left(\frac{w}{d}\right)^2 \quad . \tag{18}$$

Note that this ratio, $\frac{K}{R}$, appears in the right-hand side of Eq. (11). Consequently, Eq. (11) can be rewritten as

$$\frac{F_{r_y}}{\mu_y R} = 39\ \left(\frac{w}{d}\right)^2 \frac{\beta}{\mu_y} - 8.8 \times 10^3\ \left(\frac{w}{d}\right)^6 \left(\frac{\beta}{\mu_y}\right)^3 \quad \text{for} \quad \left|39\left(\frac{w}{d}\right)^2 \frac{\beta}{\mu_y}\right| \leq 1.5 \tag{19}$$

$$\text{and} \quad \frac{F_{r_y}}{\mu_y R} = 1 \qquad \text{for} \quad \left|39\ \left(\frac{w}{d}\right)^2 \frac{\beta}{\mu_y}\right| \geq 1.5$$

An additional simplification can be made by putting Eq. (19) into a form which is easier for the analog computer to handle. Such a form

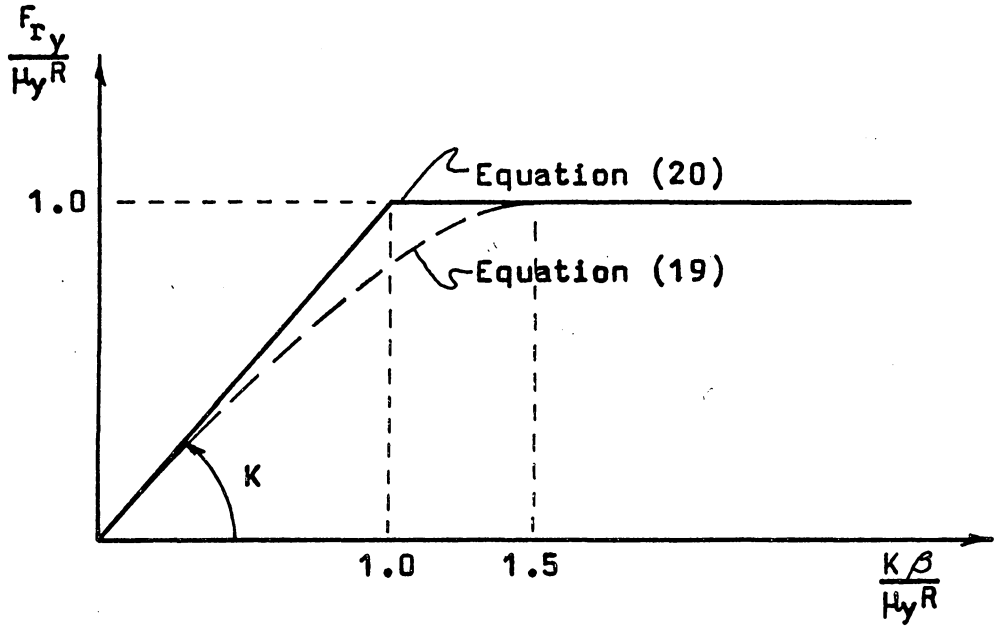

Figure 6. Cornering force approximation

is represented by the solid curve shown in Figure 6. In order to satisfy the curve in Figure 6, only the linear portion of the cornering force equation needs to be retained, and then Eq. (19) can be modified to read:

$$\frac{F_{r_y}}{\mu_y R} = 39 \left(\frac{w}{d}\right)^2 \frac{\beta}{\mu_y}, \qquad \text{for } \left|39 \left(\frac{w}{d}\right)^2 \frac{\beta}{\mu_y}\right| \leq 1 \tag{20}$$

and

$$\frac{F_{r_y}}{\mu_y R} = 1, \qquad \text{for } \left|39 \left(\frac{w}{d}\right)^2 \frac{\beta}{\mu_y}\right| \geq 1$$

But, suppose that a parameter $\bar{\beta}$ is introduced, where

$$\bar{\beta} = 39 \left(\frac{w}{d} \right)^2 \frac{\beta}{\mu_y} \quad , \qquad \text{with } -1 \leq \bar{\beta} \leq 1 \tag{21}$$

then Eq. (20) becomes

$$F_{r_y} = \bar{\beta}\, \mu_y\, R, \quad \text{for } |\bar{\beta}| \leq 1$$

and

$$F_{r_y} = \mu_y\, R, \quad \text{for } |\bar{\beta}| \geq 1 \quad . \tag{22}$$

(C) Braked Rolling.

Consider an unyawed wheel to which a braking torque, T_b, has been applied. Writing the equation of rotational motion for such a wheel about its axle, one has:

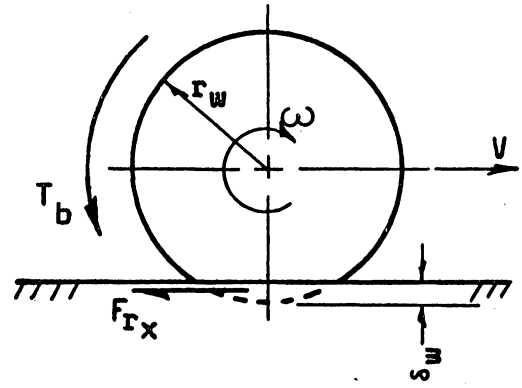

Figure 7. Forces acting on a braked wheel

$$F_{r_x} (r_w - \delta_w) - T_b = I_y \alpha \tag{23}$$

where α is the angular acceleration.

But, by definition,

$$F_{r_x} = \mu_b\, R \tag{24}$$

thus, after substituting

$$\mu_b R\, (r_w - \delta_w) - T_b = I_y \alpha \tag{25}$$

where μ_b is the coefficient of braking friction. It can be seen

from Eq. (25) that the application of a braking torque results in the wheel undergoing an angular deceleration. This causes the angular velocity to decrease. The magnitude of the braking torque, T_b, will determine how quickly the angular velocity will decrease.

When a braking torque is applied the angular velocity is decreasing faster than the corresponding translational velocity, V. This results in the inequality

$$V \neq \omega_b (r_w - \delta_w) \tag{26}$$

since the wheel is no longer rolling freely.

This situation leads to the definition of slip ratio; or as it is sometimes called, percentage slip. The slip ratio is defined as the ratio of the speed of the point of contact of the wheel to the forward speed of the wheel; or

$$s_\ell = \frac{|V_c|}{|V|} = 1 - \frac{|\omega_b (r_w - \delta_w)|}{|V|} , \tag{27}$$

where $|V_c| = |V| - |\omega_b (r_w - \delta_w)|$,

and where ω_b is the angular velocity of a braked wheel. (Zero slip ($s_\ell = 0$) represents the free rolling of the wheel, while 100 percent slip ($s_\ell = 1.0$) represents a locked, non-rotating wheel.)

Applying a braking torque to a rolling wheel causes the wheel to slip. This, in turn, causes the coefficient of friction to change.

Figure 8 indicates how the coefficient of braking friction μ_b varies with the slip ratio, s_l. When $s_l = 0$, the coefficient of braking friction reduces to, μ_r, the coefficient of rolling friction; and when $s_l = 1.0$, it becomes the coefficient of skidding friction, μ_s.

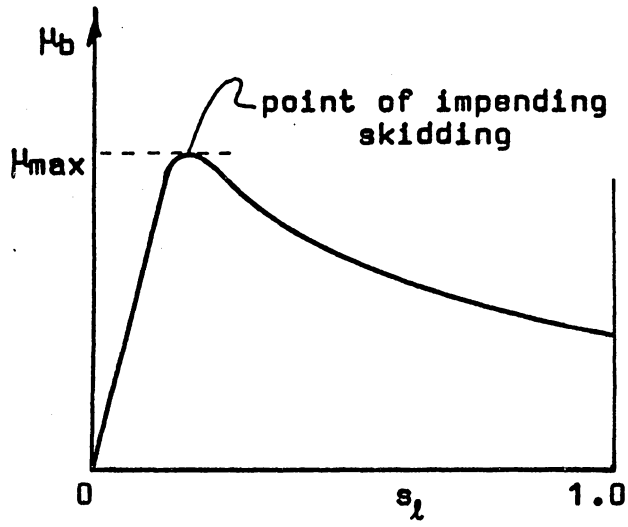

Figure 8. Coefficient of braking friction as a function of slip ratio

To understand how the slip ratio affects the coefficient of braking friction consider the application of a small braking torque, T_{b_1}, to a freely rolling wheel. Initially T_{b_1} will be greater than $\mu_b R (r_w - \delta_w)$ and the wheel will decelerate until the torques or moments on the wheel reach equilibrium. Therefore, Eq. (25) reduces to:

$$T_{b_1} = \mu_{b_1} R (r_w - \delta_w) . \quad (28)$$

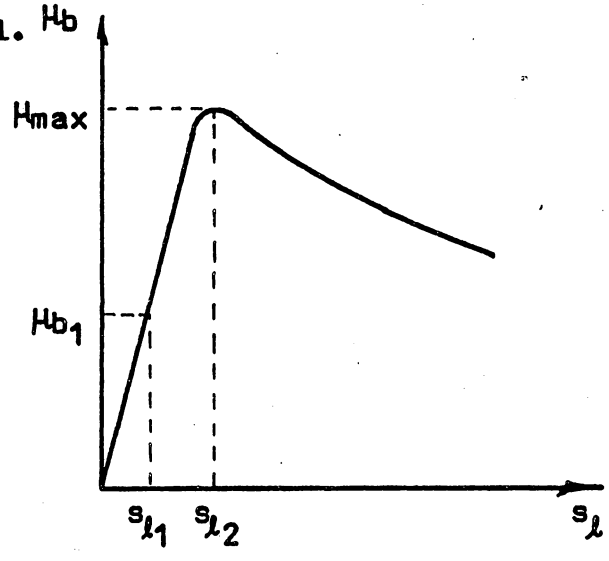

Figure 9. Coefficient of braking friction for small slip ratios

Furthermore, if ω_{b_1} is defined as the angular velocity at which the torques are equal, Eq. (27) reduces to

$$s_{\ell_1} = 1 - \frac{\omega_{b_1}(r_w - \delta_w)}{|V|} \quad . \tag{29}$$

Thus, by considering Eqs. (28) and (29), in conjunction with Figure 9, it can be seen that for each value of braking torque there is a corresponding value of the coefficient of braking friction.

Now, if the magnitude of the braking torque is slowly, but continuously increased, the slip ratio which corresponds to the coefficient of maximum braking friction, μ_{max}, will eventually be attained. At this slip ratio Eq. (25) becomes

$$T_{b_2} = \mu_{max} R(r_w - \delta_w) \quad . \tag{30}$$

However, if the braking torque is increased further, to a value greater than T_{b_2}, the slip ratio will correspondingly increase; but μ_b will decrease and Eq. (25) will reduce to the inequality

$$T_b > \mu_b R (r_w - \delta_w) \quad . \tag{31}$$

This means that the wheel will continue to decelerate until it ceases to rotate. The condition of a wheel translating without rotating is called a full skid . Thus, it can be seen why μ_{max} is referred to as the point of impending skidding, as indicated in Figure 8.

If a wheel is to operate at maximum braking efficiency it should operate at the slip ratio corresponding to μ_{max}. However, once the slip ratio has become larger than that corresponding to μ_{max}, then the wheel will begin to skid.

This situation has lead to the use of automatic braking devices which employ anti-skid units in their operation. Briefly, these automatic braking devices release the brake pressure whenever the point of impending skidding has been passed and wheel spindown is occurring; then, reapplying the brake pressure when the wheel has spun up to some predetermined angular velocity corresponding to a slip ratio above μ_{max}. Thus, the automatic braking device causes the braking system to cycle through periods where the brake pressure is alternately applied and released. The purpose of this cyclic variation is to maintain a slip ratio in the vicinity of μ_{max}.

As a consequence of this cyclic operation, and since the wheel does not remain at μ_{max} during the entire braking cycle, the coefficient of average braking coefficient, μ_{av} (as shown in Figure 10) will be considered as representative of the true value of the coefficient of braking friction during maximum braking. Measurements have shown that, to a fair approximation,

$$\mu_{av} \approx 0.9\, \mu_{max} \quad . \tag{32}$$

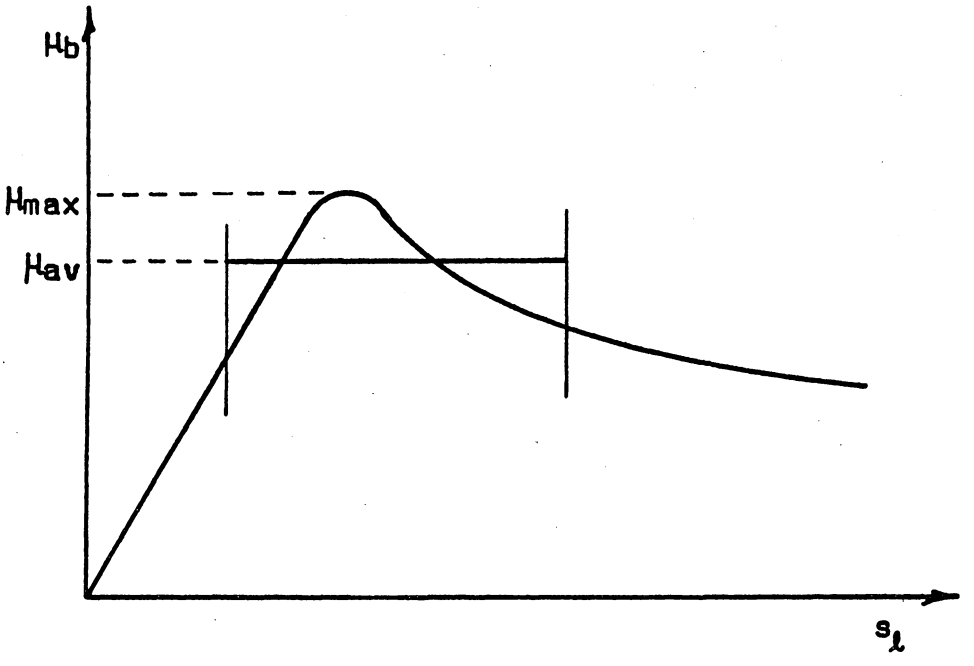

Figure 10. Relation between μ_{max} and μ_{av}

For dry surfaces the coefficient of maximum braking friction is primarily a function of tire pressure

$$\mu_{max} = 0.93 - 0.00157\ p \tag{33}$$

Equation (33) is an empirical relation which will provide the coefficient of maximum braking friction for modern aircraft tires. By combining Eqs. (32) and (33) the following useful relation is obtained

$$\mu_{av} = 0.84 - 0.00141\ p \tag{34}$$

where p has the units of pounds per square inch.

If, after the brakes are applied, the wheel is allowed to spin down until it stops rotating, then the wheel is described as being in a full skid. This situation is equivalent to simple sliding friction, for which there is a single frictional drag force acting in a direction opposite to the direction of motion regardless of the orientation of the wheel. For dry runways the coefficient of skidding friction, μ_s, is a function of tire pressure and aircraft speed. As stated earlier, the coefficient of skidding friction may be considered to be equivalent to the coefficient of side friction. Consequently, values of μ_s may be obtained by using Figure 5 and Eqs. (12) and (13).

The cornering force, F_{r_y}, acting on a tire is influenced by changes in the slip ratio. Reference 3 states that during braking, the cornering forces acting on a yawed tire are greatly reduced. However, the results of Reference 3 are incomplete - it was not determined whether the reduction in cornering force is caused by a decrease in cornering power, by a decrease in the coefficient of side friction, or by a decrease of both. However, the data presented in Reference 3 seems to indicate that the cornering force is reduced by approximately 80 percent during braking, and that braking has a greater effect upon the coefficient of side friction. Therefore, for the purposes of this study it will be assumed that

$$\mu_{y_b} = \frac{\mu_y}{5} .$$

Thus, during braking, the coefficient of side friction will be assumed to be that given by the above equation for μ_{y_b}.

(D) Wet Runways.

A consideration of the motion of a wheel over a wet or slushy runway is not as simple as that for dry runways. This is primarily due to inconsistencies in the depth of the fluid covering the runway, and the existence of hydrodynamic pressures - such as the hydrodynamic lift - which can cause tire hydroplaning at high speeds.

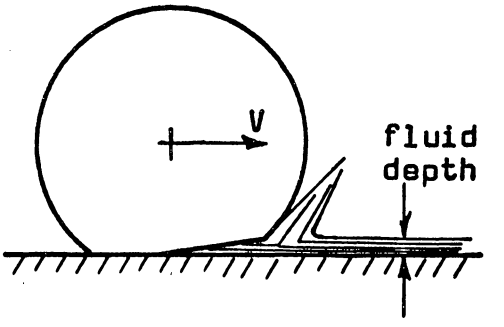

Figure 11. Wheel rolling on a wet runway

Consider a tire moving over a fluid-covered runway. As the tire moves forward, at a velocity V, a wedge of fluid is forced under the tire as indicated in Figure 11. Thus, only a part of the load on the tire is supported by the runway; the remainder of the load is supported by the fluid. It is the existence of this hydrodynamic lift which results in lower friction coefficients on wet surfaces. When this wedge of fluid is forced all the way to the rear edge of the tire's supporting surface, the tire is lifted from the runway

surface and is supported fully by hydrodynamic pressure. This phenomena, where a tire is supported by a fluid, is called hydroplaning .

The present investigation will avoid the problem of skidding under the conditions of hydroplaning for several reasons. First, hydroplaning occurs only at high speeds where the aircraft's aerodynamic stability is still effective and where aerodynamic control is used. For example, according to an empirical relation given in Reference 4, a tire with an inflation pressure of 200 lb/in^2 will not hydroplane at speeds below 215 feet/second. Second, Reference 4 states that a minimum fluid depth of 0.17 inches is required for hydroplaning on a completely smooth surface, and a minimum fluid depth of 0.42 inches on a grooved surface. This suggests a value of from 0.2 to 0.3 inches of water for the average concrete runway. Third, previous investigations of hydroplaning have been limited to unyawed wheels; there is no available information describing the hydroplaning behavior of yawed tires.

From the above discussion and for wet runway conditions, this study will be limited to water depths less than those necessary for hydroplaning. Furthermore, since the values of the friction coefficients are influenced by the depth of standing water, it will be assumed that the water depth on the runway is constant. This, in turn, permits the assumption that the friction coefficients are

constants for a wet runway. Typical values of the coefficient of friction, for wet runway surfaces, are shown in Figures 12 and 13; these are represented as functions of forward velocity and tire pressure.

(E) Ice and Snow-covered Runways.

Ice and snow-covered runways are characterized by their inability to produce large frictional forces. The friction coefficients for tires on ice and snow can usually be considered as constants, since they are practically independent of tire pressure and forward velocity.

For frozen, ice-covered surfaces, the coefficient of maximum braking friction, and the coefficient of skidding friction are, respectively, 0.18 and 0.10. These values may be considered as constants for all conditions. Note that these values are applicable only at temperatures below freezing.

The values of friction coefficients for snow-covered surfaces are more difficult to define since these quantities vary greatly with the temperature, the wetness of the snow, and the condition of the subsurface. In general, the coefficient of maximum braking friction has values ranging from 0.25 to 0.37; and the coefficient of skidding friction varies from 0.15 to 0.23. The friction coefficients are lower for below freezing temperatures, dry snow, and

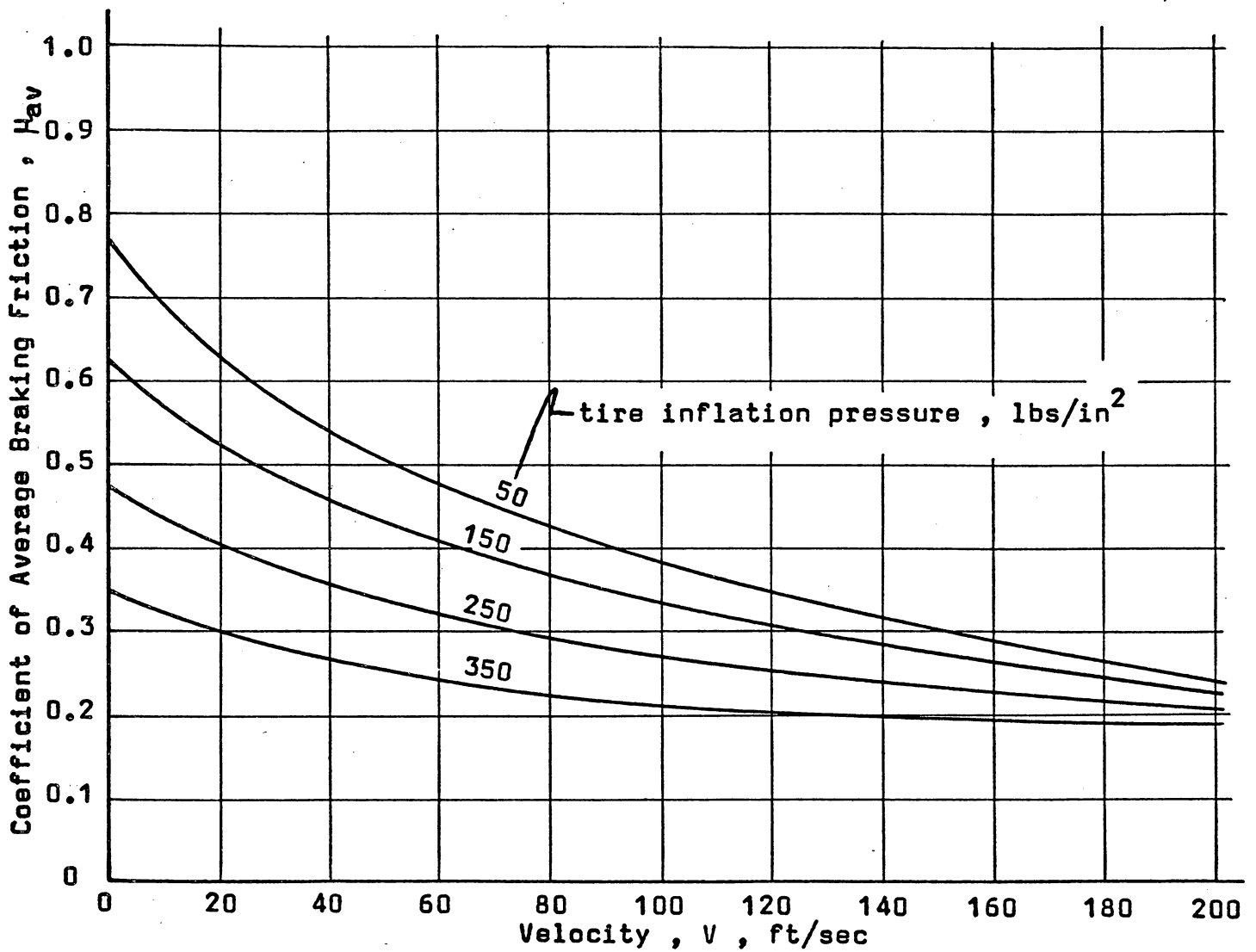

Figure 12. Coefficient of average braking friction on a wet runway as a function of pressure and velocity

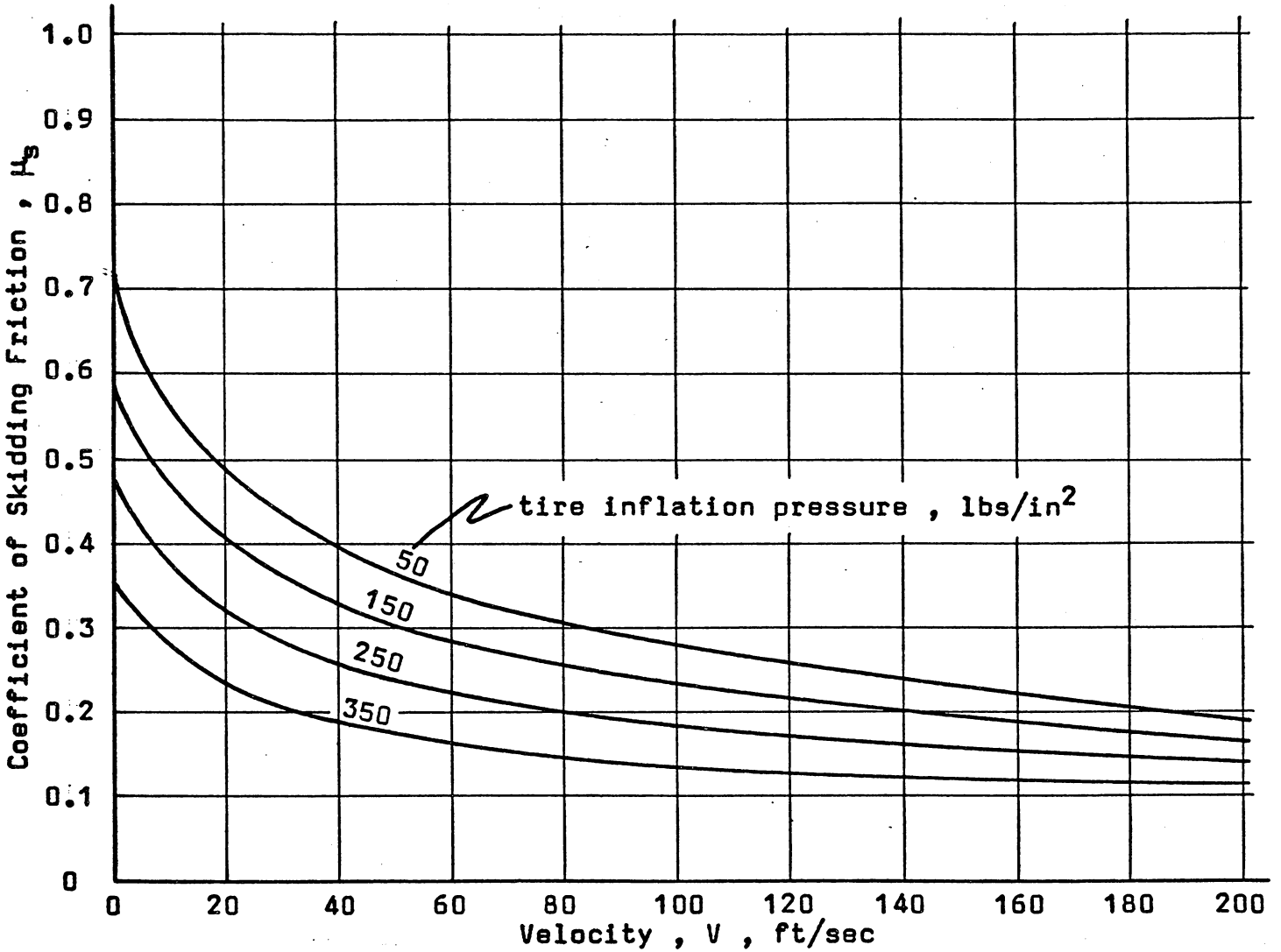

Figure 13. Coefficient of skidding friction on a wet runway as a function of pressure and velocity

icy subsurfaces; and are higher for above-freezing temperatures, wet snow, and bare subsurfaces.

(F) Aerodynamic Forces.

The lift force, L, is defined as

$$L = \frac{1}{2} C_L \rho V^2 S \quad . \tag{35}$$

For an airplane during the landing ground roll, this force is normal to the runway surface, thus it acts in the negative z-direction. The lift coefficient, C_L, is known to be a function of Reynolds number and of angle of attack. In this analysis, it will be assumed that the runway is flat and level and that there are no oscillations due to landing gear compression and relaxation. Hence, the airplane's attitude in pitch and its angle of attack will be constant. Therefore, if the Reynolds number effects are neglected, the lift coefficient is essentially constant during the ground roll after touchdown. (Note: it is assumed that mechanical devices such as flaps, spoilers, etc., are not moved during the landing roll.)

Therefore, for all practical purposes the lift acting on the aircraft is determined only by the aircraft's forward speed, V, and the angle of sideslip, β. In order to account for the effects of sideslip, and to simplify the equations of motion later, it will be assumed that

$$L = \frac{1}{2} C_L \rho u^2 S \qquad (36)$$

where u is the velocity component in the airplane's x-direction. Thus, when the aircraft is traveling straight ahead, $u = V$ and Eq. (36) is equivalent to Eq. (35). Also, since $u = V \cos \beta$, in general, the lift force is reduced by the amount $\cos^2 \beta$ when the airplane is yawed. This variation is only an approximation and is used to make the computations easier to handle in solving the equations of motion.

The drag force, D, is defined as

$$D = \frac{1}{2} C_D \rho V^2 S \quad .$$

For an airplane during the landing roll, this force acts parallel to the plane of the runway. However, as with the lift force, it will be assumed that

$$D = \frac{1}{2} C_D \rho u^2 S \qquad (37)$$

and that the drag force acts in the airplane's negative x-direction. It will be assumed here that the drag coefficient is a constant.

Next, the aerodynamic side force, Y, is defined as

$$Y = \frac{1}{2} C_y \rho V^2 S$$

where C_y is the aerodynamic side force coefficient. The side force

is considered to act in the airplane's positive y-direction. For the case of ground roll, with all wheels on the ground, the side force coefficient is a function of the angle of sideslip, β, only, or

$$C_y = \frac{\partial C_y}{\partial \beta} \beta = C_{y_\beta} \beta \quad ,$$

where C_{y_β} is referred to as the side force derivative. Thus, the aerodynamic side force is expressed as

$$Y = \frac{1}{2} C_{y_\beta} \beta \rho V^2 S \quad . \tag{38}$$

(G) Aerodynamic Moments.

For the purposes of this thesis, the aerodynamic moments, rolling, pitching, and yawing moments, respectively, acting on an airplane are defined as

$$L_a = \frac{1}{2} C_\ell \rho V^2 S b$$

$$M_a = \frac{1}{2} C_m \rho u^2 S b$$

and

$$N_a = \frac{1}{2} C_n \rho V^2 S b \quad .$$

First, consider the rolling moment coefficient, C_ℓ . For an airplane during its ground roll, the rolling moment coefficient is a function of the angle of sideslip, β, the yawing rate, r, and the

aileron deflection, δ_a. Thus, in terms of the stability derivatives, C_{ℓ_β}, C_{ℓ_r}, and $C_{\ell_{\delta_a}}$,

$$L_a = \frac{1}{2} \left(C_{\ell_\beta} \beta + C_{\ell_r} r + C_{\ell_{\delta_a}} \delta_a \right) \rho V^2 S b \quad .$$

Or, if the ailerons are considered to be fixed,

$$L_a = \frac{1}{2} \left(C_{\ell_\beta} \beta + C_{\ell_r} r \right) \rho V^2 S b \quad . \tag{39}$$

Similarly, for the pitching moment, M_a, during the landing roll,

$$M_a = M_a \quad (\alpha_L, \delta_e) \quad .$$

Thus, in terms of the stability derivatives,

$$M_a = \frac{1}{2} \left(C_{m_\alpha} \alpha_L + C_{m_{\delta_e}} \delta_e \right) \rho u^2 S b \quad . \tag{40}$$

Note that for the product $C_{m_\alpha} \alpha_L$ is a constant during landing.

For the yawing moment, N_a, where

$$N_a = N_a (\beta, r, \delta_r) \quad ,$$

the aerodynamic yawing moment is given by

$$N_a = \frac{1}{2} \left(C_{n_\beta} \beta + C_{n_r} r + C_{n_{\delta_r}} \delta_r \right) \rho V^2 S b \quad . \tag{41}$$

It is assumed that all aerodynamic coefficients have linear variations and, therefore, are constants in the equations of motion. It is also assumed here that all aerodynamic coefficients are independent of Reynolds number.

(H) Gravity Force.

The vehicle's landing weight, defined as

$$W = m\,g$$

acts in the positive z-direction and is a constant.

(I) Thrust.

The thrust force, T, is aligned with the x-axis of the vehicle and acts in the positive x-direction. This is true except for the case of thrust reversal, when the thrust acts in the negative x-direction. However, in the computations leading to the solution of the equations of motion, it is assumed that thrust is negligible during the landing roll.

(J) Axis System.

As stated previously, the equations of motion are written relative to a set of body axes. The orientation of this axis system is shown in Figure 14.

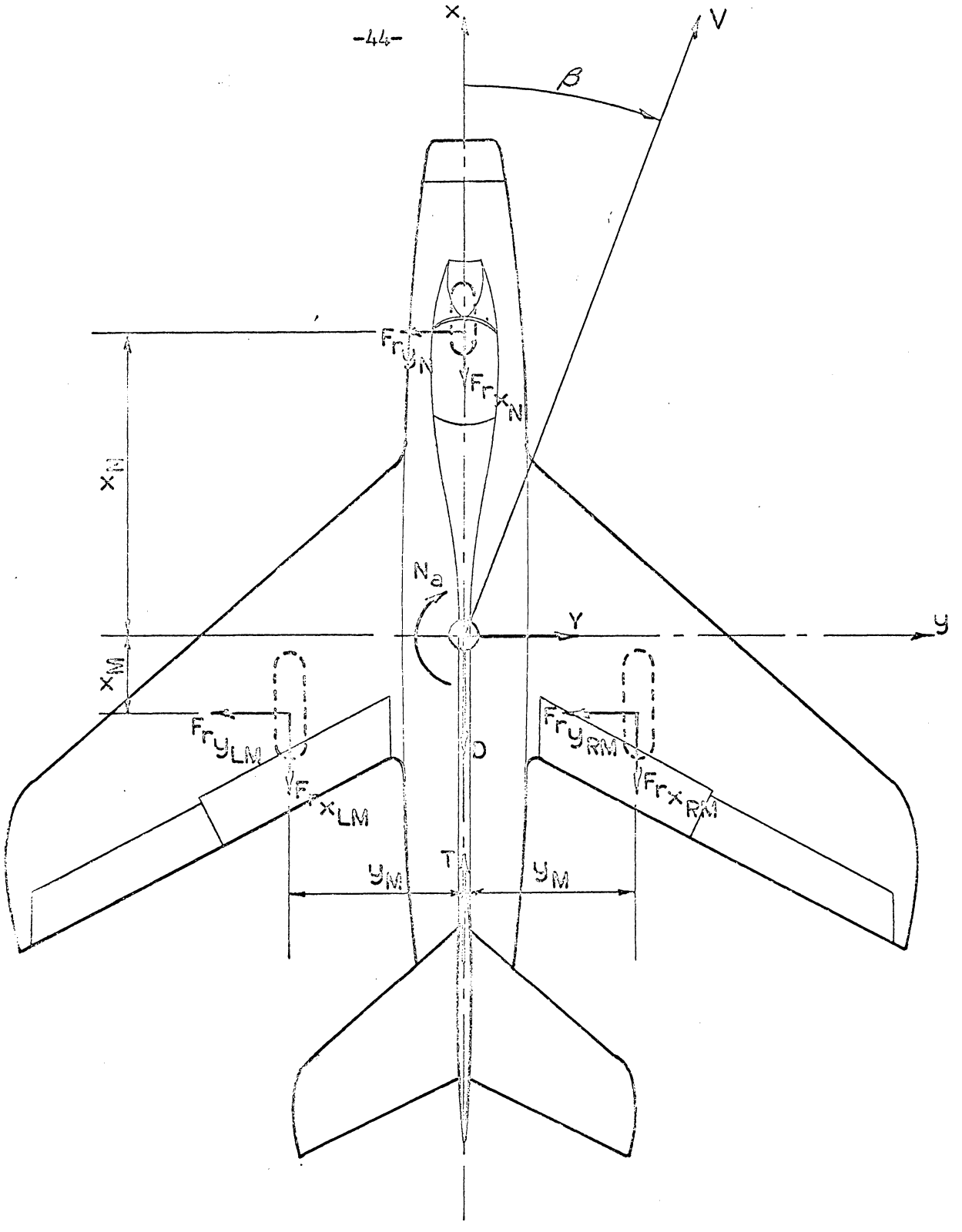

Figure 14a. Forces acting on an airplane during the landing roll

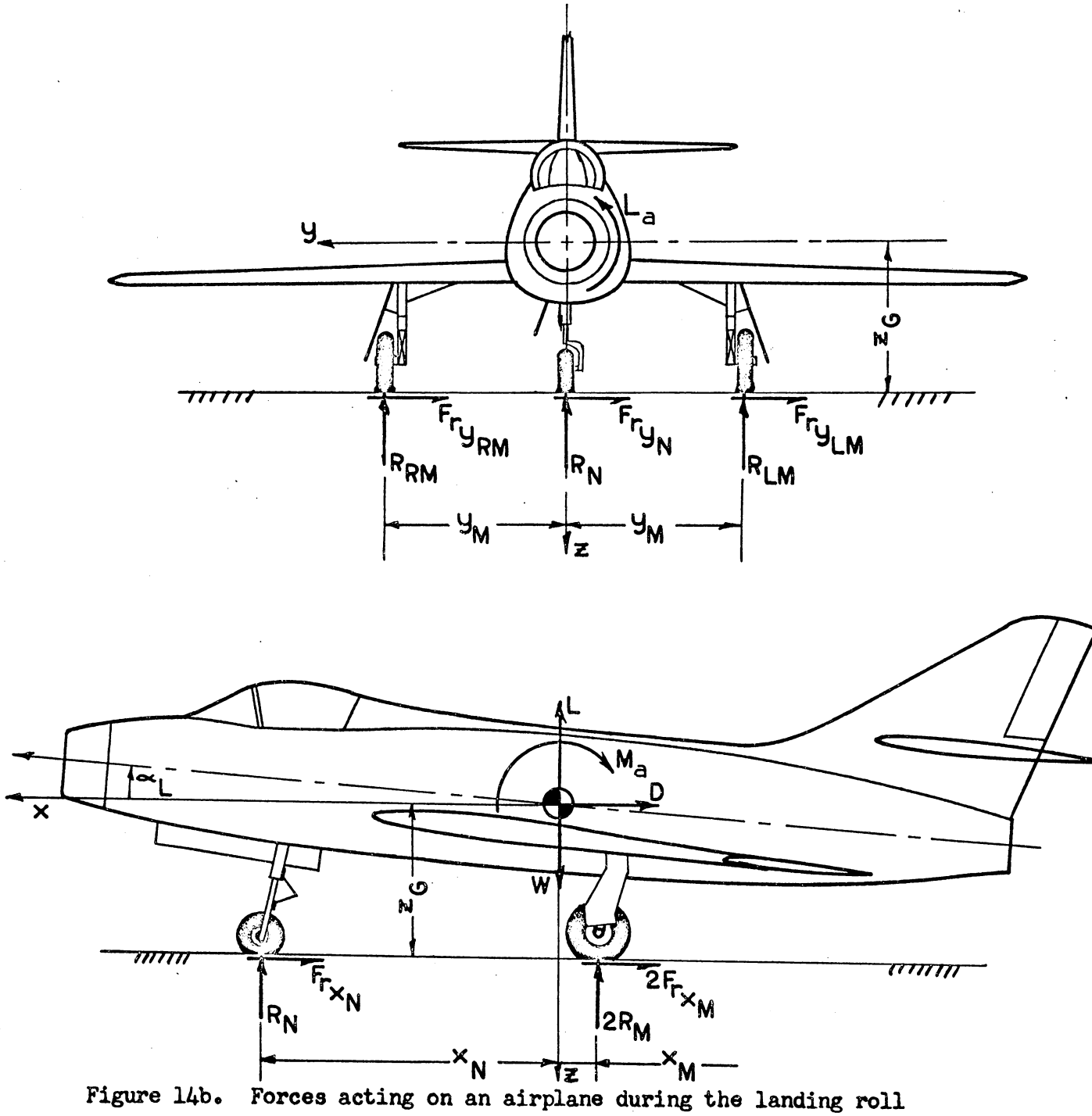

Figure 14b. Forces acting on an airplane during the landing roll

(K) Equations of Motion for an Airplane during the Landing Roll.

Summing the forces and moments acting on an airplane on the runway leads to the following equations of motion:

$$\sum F_x = T - D - F_{r_{x_N}} - F_{r_{x_{LM}}} - F_{r_{x_{RM}}} = m(\dot{u} - vr) \tag{42}$$

$$\sum F_y = Y - F_{r_{y_N}} - F_{r_{y_{LM}}} - F_{r_{y_{RM}}} = m(\dot{v} + ur) \tag{43}$$

$$\sum F_z = W - L - R_N - R_{LM} - R_{RM} = 0 \tag{44}$$

$$\sum L = L_a + (R_{LM} - R_{RM})\, y_M + (F_{r_{y_N}} + F_{r_{y_{LM}}} + F_{r_{y_{RM}}}) z_G = -I_{xz}\dot{r} \tag{45}$$

$$\sum M = M_a + R_N x_N - (R_{LM} + R_{RM})\, x_M - (F_{r_{x_N}} + F_{r_{x_{LM}}} + F_{r_{x_{RM}}})\, z_G = - I_{xz}\, r^2 \tag{46}$$

and

$$\sum N = N_a - F_{r_{y_N}}\, x_N + (F_{r_{y_{LM}}} + F_{r_{y_{RM}}})\, x_M - (F_{r_{x_{LM}}} - F_{r_{x_{RM}}})\, y_M = I_z\, \dot{r}\,. \tag{47}$$

It can be seen from Eq. (22) that $\frac{F_{r_y}}{R} \leq \mu_y$. Thus, since μ_y is very small, the rolling moments due to the landing gear side forces will be neglected. It will also be assumed that the tire properties are the same for both main tires, or that

$$\mu_{x_{LM}} = \mu_{x_{RM}} = \mu_{x_M}$$

$$\mu_{y_{LM}} = \mu_{y_{RM}} = \mu_{y_M}$$

$$\bar{\beta}_{LM} = \bar{\beta}_{RM} = \bar{\beta}_M$$

$$R_{LM} + R_{RM} = 2R_M$$

and

$$R_{LM} - R_{RM} = \Delta R_M \ .$$

Using these assumptions and substituting into the equations of motion the following set is obtained:

The "drag" equation;

$$T - \frac{1}{2} C_D \rho u^2 S - \mu_{x_N} R_N - 2 \mu_{x_M} R_M = m(\dot{u} - vr) \ , \qquad (48)$$

the side force equation;

$$\frac{1}{2} C_{y_\beta} \beta \rho V^2 S - \bar{\beta}_N \mu_{y_N} R_N - 2\bar{\beta}_M \mu_{y_M} R_M = m(\dot{v} + ur) \qquad (49)$$

the "lift" equation;

$$R_N + 2R_M = W - \frac{1}{2} C_L \rho u^2 S \qquad (50)$$

the rolling moment equation;

$$\Delta R_M = \frac{1}{y_M} \left[-I_{xz} \dot{r} - \frac{1}{2} (C_{\ell_\beta} \beta + C_{\ell_r} r + C_{\ell_{\delta_a}} \delta_a) \rho V^2 S b \right] \qquad (51)$$

the pitching moment equation;

$$R_N(x_N - \mu_{x_N} z_G) - 2R_M(x_M + \mu_{x_M} z_G) =$$
$$- \mu I_{xz} r^2 - \frac{1}{2} (C_{m_\alpha} \alpha_L + C_{m_{\delta_e}} \delta_e) \rho u^2 S b \qquad (52)$$

and, the yawing moment equation;

$$\frac{1}{2}\left(C_{n_\beta}\beta + C_{n_r} r + C_{n_{\delta_r}} \delta_r\right) \rho V^2 S b - \bar{\beta}_N \mu_{y_N} R_N x_N + 2\bar{\beta}_M \mu_{y_M} R_M x_M - \Delta R_M \mu_{x_M} y_M = I_z \dot{r} \quad . \tag{53}$$

These equations are applicable only if the landing gear wheels are in contact with the runway.

For the purposes of analysis it is desirable to rearrange Eqs. (50) and (52). Solving these expressions for $2R_M$ and R_N gives,

$$R_N = \frac{1}{k}\left[-I_{xz} r^2 + W\left(x_M + \mu_{x_M} z_G\right) - \frac{1}{2}\left[\left(C_{m_\alpha}\alpha_L + C_{m_{\delta_e}} \delta_e\right) b + C_L\left(x_M + \mu_{x_M} z_G\right)\right] \rho u^2 S\right] \tag{54}$$

and

$$2R_M = \frac{1}{k}\left[I_{xz} r^2 + W\left(x_N - \mu_{x_N} z_G\right) + \frac{1}{2}\left[\left(C_{m_\alpha}\alpha_L + C_{m_{\delta_e}} \delta_e\right) b + C_L\left(x_N - \mu_{x_N} z_G\right)\right] \rho u^2 S\right] \tag{55}$$

where

$$k = x_M + x_N + \left(\mu_{x_M} - \mu_{x_N}\right) z_G \quad . \tag{56}$$

It is noted that Eqs. (54) and (55) can be simplified further. Consider the first two terms on the right hand sides of these equations; for most modern aircraft,

$$\frac{I_{xz}}{W} < \frac{1}{12} \text{ ft-sec}^2$$

and if it is assumed that

$$r < 1/3 \text{ rad/sec}$$

and

$$x_M + \mu_{x_M} z_G > 1 \text{ ft}$$

then

$$\frac{I_{xz}}{W} r^2 < \frac{1}{96} \ll 1 \ll (x_M + \mu_{x_M} z_G),$$

hence

$$I_{xz} r^2 \ll W(x_M + \mu_{x_M} z_G) \quad .$$

Also, since

$$(x_M + \mu_{x_M} z_G) \ll (x_N - \mu_{x_N} z_G)$$

then

$$I_{xz} r^2 \ll W(x_N - \mu_{x_N} z_G) \quad ,$$

therefore Eqs. (54) and (55) may be rewritten as:

$$R_N = \frac{1}{k}\left[W(x_M + \mu_{x_M} z_G) - \right.$$

$$\left. \frac{1}{2}\left[b(C_{m_\alpha} \alpha_L + C_{m_{\delta_e}} \delta_e) + C_L(x_M + \mu_{x_M} z_G)\right] \rho u^2 S \right] \qquad (57)$$

and

$$2R_M = \frac{1}{k}\left[W(x_N - \mu_{x_N} z_G) + \right.$$

$$\left. \frac{1}{2}\left[b(C_{m_\alpha} \alpha_L + C_{m_{\delta_e}} \delta_e) + C_L(x_N - \mu_{x_N} z_G)\right] \rho u^2 S \right] \quad . \qquad (58)$$

Equations (51), (57), and (58) are expressions for the landing gear reactions; and they will be substituted into Eqs. (48), (49), and (53). Making the proper substitutions into Eq. (48), the drag equation becomes

$$T - \frac{W}{k}\left(\mu_{x_N} x_M + \mu_{x_M} x_N\right) + \frac{C_L}{2k}\left(\mu_{x_N} x_M + \mu_{x_M} x_N\right) \rho u^2 S -$$

$$\frac{1}{2} C_D \rho u^2 S - \frac{b}{2k}\left(C_{m_\alpha} \alpha_L + C_{m_{\delta_e}} \delta_e\right)\left(\mu_{x_M} - \mu_{x_N}\right) \rho u^2 S =$$

$$m(\dot{u} - vr) \quad . \tag{59}$$

Substituting into Eq. (49), the side force equation becomes:

$$\frac{1}{2} C_{y_\beta} \beta \rho V^2 S - \frac{W}{k}\left[\bar{\beta}_N \mu_{y_N}\left(x_M - \mu_{x_M} z_G\right) + \bar{\beta}_M \mu_{y_M}\left(x_N - \mu_{x_N} z_G\right)\right] +$$

$$\frac{C_L}{2k}\left[\bar{\beta}_N \mu_{y_N}\left(x_M + \mu_{x_M} z_G\right) + \bar{\beta}_M \mu_{y_M}\left(x_N - \mu_{x_N} z_G\right)\right] \rho u^2 S -$$

$$\frac{b}{2k}\left(C_{m_\alpha} \alpha_L + C_{m_{\delta_e}} \delta_e\right)\left(\bar{\beta}_M \mu_{y_M} - \bar{\beta}_N \mu_{y_N}\right) \rho u^2 S = m(\dot{v} + ur) \quad . \tag{60}$$

and after substituting into Eq. (53), the yawing moment equation is found to be

$$\frac{1}{2}\left[(C_{n_\beta} + \mu_{x_M} C_{l_\beta})\beta + (C_{n_r} + \mu_{x_M} C_{l_r})\, r + C_{n_{\delta_r}} \delta_r\right] \rho V^2 S b +$$

$$\frac{w}{k}\left[\bar{\beta}_M \mu_{y_M} x_M (x_N - \mu_{x_N} z_G) - \bar{\beta}_N \mu_{y_N} x_N (x_M + \mu_{x_M} z_G)\right] -$$

$$\frac{C_L}{2k}\left[\bar{\beta}_M \mu_{y_M} x_M (x_N - \mu_{x_N} z_G) - \bar{\beta}_N \mu_{y_N} x_N (x_M + \mu_{x_M} z_G)\right] \rho u^2 S +$$

$$\frac{b}{2k}(C_{m_\alpha} \alpha_L + C_{m_{\delta_e}} \delta_e)(\bar{\beta}_M \mu_{y_M} x_M + \bar{\beta}_N \mu_{y_N} x_N) \rho u^2 S = I_z \dot{r} \quad . \quad (61)$$

It should be noted that for the right-hand side of Eq. (61), it was assumed that

$$\mu_{x_M} I_{xz} \ll I_z \quad .$$

Equations (59), (60), and (61) are the airplane equations of motion during the landing roll. However, to obtain a solution to these equations, on the analog computer available, one additional assumption must be made. This concerns the variable products βV^2, rV^2, and $\delta_r V^2$ which appear on the left-hand side of Eqs. (60) and (61). The forward speed component, u, and the side speed component, v, are expressed by

$$u = V \cos \beta \approx V \quad (62)$$

and

$$v = V \sin \beta \approx V\beta \quad (63)$$

where it is assumed that β is a small angle; so, using Eqs. (62) and

(63) to modify the variable products βV^2, rV^2, and $\delta_r V^2$, one obtains

$$\beta V^2 = V(V\beta) = V\, v \tag{64}$$

$$rV^2 = V(Vr) = V\, ur \tag{65}$$

and

$$\delta_r V^2 = \delta_r\, u^2 \quad . \tag{66}$$

Thus, the variables βV^2 and rV^2 will be replaced by V v and V ur. For these two terms it will be assumed that v and ur are the variables, and that V is a constant. An average value of the velocity, V, will be used in the computer program. The variable $\delta_r V^2$ will simply be replaced by the variable $\delta_r u^2$. It should be noted that this last assumption affects only certain aerodynamic terms in Eqs. (60) and (61).

After substituting Eqs. (64), (65), and (66) into the equations of motion and rearranging, the drag equation, the side force equation, and the yawing moment equation, respectively, are

$$\dot{u} = vr - C_1\, u^2 - C_2 \tag{67}$$

$$\dot{v} = -ur + C_3 v - C_4\, \bar{\beta}_M - C_5\, \bar{\beta}_N + C_6\, \bar{\beta}_M\, u^2 + C_7\, \bar{\beta}_N\, u^2 \tag{68}$$

and

$$\dot{r} = C_8 v + C_9 ur + C_{10}\, \bar{\beta}_M - C_{11}\, \bar{\beta}_N - C_{12}\, \bar{\beta}_M\, u^2 + C_{13}\, \bar{\beta}_N\, u^2 + C_{14}\, \delta_r\, u^2 \quad . \tag{69}$$

The coefficients C_1 through C_{14} are constants and are given by the following relations:

$$C_1 = \frac{\rho S}{2km}\left[k\, C_D + b(C_{m_\alpha}\,\alpha_L + C_{m_{\delta_e}}\,\delta_e)(\mu_{x_M} - \mu_{x_N}) - C_L(\mu_{x_N} x_M + \mu_{x_M} x_N)\right]$$

$$C_2 = \frac{g}{k}\,(\mu_{x_N} x_M + \mu_{x_M} x_N) - \frac{T}{m}$$

$$C_3 = \frac{1}{2m}\, C_{y_\beta}\, \rho\, V\, S$$

$$C_4 = \frac{g}{k}\, \mu_{y_M}\, (x_N - \mu_{x_N} z_G)$$

$$C_5 = \frac{g}{k}\, \mu_{y_N}\, (x_M + \mu_{x_M} z_G)$$

$$C_6 = \frac{\rho S}{2km}\, \mu_{y_M}\left[C_L(x_N - \mu_{x_N} z_G) - b(C_{m_\alpha}\alpha_L + C_{m_{\delta_e}}\,\delta_e)\right]$$

$$C_7 = \frac{\rho S}{2km}\, \mu_{y_N}\left[C_L(x_M + \mu_{x_M} z_G) + b(C_{m_\alpha}\alpha_L + C_{m_{\delta_e}}\,\delta_e)\right]$$

$$C_8 = \frac{\rho V S b}{2I_z}\, (C_{n_\beta} + \mu_{x_M}\, C_{\ell_\beta})$$

$$C_9 = \frac{\rho V S b}{2I_z}\, (C_{n_r} + \mu_{x_M}\, C_{\ell_r})$$

$$C_{10} = \frac{w}{kI_z}\, \mu_{y_M}\, x_M\, (x_N - \mu_{x_N} z_G)$$

$$C_{11} = \frac{W}{kI_z} \mu_{y_N} x_N (x_M + \mu_{x_M} z_G)$$

$$C_{12} = \frac{\rho S}{2kI_z} \mu_{y_M} x_M \left[C_L(x_N - \mu_{x_N} z_G) - b(C_{m_\alpha} \alpha_L + C_{m_{\delta_e}} \delta_e) \right]$$

$$C_{13} = \frac{\rho S}{2kI_z} \mu_{y_N} x_N \left[C_L(x_M + \mu_{x_M} z_G) + b(C_{m_\alpha} \alpha_L + C_{m_{\delta_e}} \delta_e) \right]$$

$$C_{14} = \frac{1}{2I_z} C_{n_{\delta_r}} \rho S b$$

The three simultaneous equations, (67), (68) and (69) describe the motion of an airplane with the nosewheel locked during the landing roll. This set of equations can be solved for the variables u, v, and r.

However, the motion of the aircraft during the landing roll can be more easily analyzed if the variables, β, ψ, and $\dot{\psi}$ are considered in place of the variables u, v, and r. Figure 14 shows that the angle of sideslip β is given by

$$\beta = \text{arc tangent } \frac{v}{u} \quad . \tag{70}$$

But, if it is assumed that β is a small angle, then Eq. (70) reduces to

$$\beta \approx \frac{v}{u} \quad . \tag{71}$$

In addition, the relation between β and $\bar{\beta}$ was previously given by Eq. (21). Hence, by applying Eq. (21), expressions for the variables $\bar{\beta}_M$ and $\bar{\beta}_N$ are obtained as

$$\bar{\beta}_M = \frac{39}{\mu_{y_M}} \left(\frac{w}{d} \right)_M^2 \beta \qquad \text{where} \quad -1 \leq \bar{\beta}_M \leq +1 \tag{72}$$

and

$$\bar{\beta}_N = \frac{39}{\mu_{y_N}} \left(\frac{w}{d} \right)_N^2 \beta \qquad \text{where} \quad -1 \leq \bar{\beta}_N \leq +1 \ . \tag{73}$$

Note that the variables $\bar{\beta}_M$ and $\bar{\beta}_N$ have a limiting value of ± 1.

Furthermore, the kinematic relation

$$r = \dot{\psi} \tag{74}$$

applies during the landing roll. The yawing angle, ψ, can be obtained from Eq. (74) by integration, or

$$\psi = \int \dot{\psi} \, dt = \int r \, dt \tag{75}$$

As stated previously, the equation set (67), (68), and (69) describes airplane motion during the landing roll only if the nosewheel is locked. If the nosewheel is freed, then another variable is introduced into the problem and a fourth equation is necessary if a solution is to be obtained. This (fourth) equation is an expression describing the steering of the nosewheel.

(L) Steering Equation.

In order to write the equation of motion for a nosewheel, rotating freely about its steering axis, the forces acting on the nosewheel must be evaluated. According to Reference 5, the only force which produces a moment about the steering axis is the cornering force, F_{r_y}. The cornering force gives rise to a moment since it is displaced from the steering axis by the pneumatic castor (q) and by the physical offset (ϵ) of the steering axis as shown in Figure 15. Hence, the moment acting on the nosewheel about its steering axis is

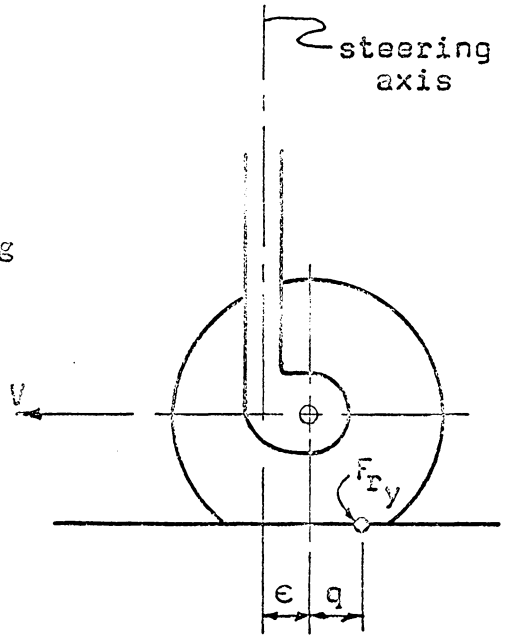

Figure 15. Forces acting on a freely swiveling nosewheel

$$M_N = F_{r_y}(\epsilon + q) = F_{r_y}\epsilon + F_{r_y} q \quad .$$

Or, since $T_z = F_{r_y} q$, then

$$M_N = F_{r_y}\epsilon + T_z \quad . \tag{76}$$

The cornering force, F_{r_y}, has been discussed previously; also an empirical expression for the self-aligning torque, T_z, has been found in Reference 2.

Thus, by summing the moments acting about the steering axis of a freely swiveling nosewheel the equation of motion is found to be

$$I_N \ddot{\delta}_N + M_N = 0$$

or,

$$\ddot{\delta}_N = \frac{\epsilon}{I_N} F_{r_y} + \frac{T_z}{I_N} \quad , \tag{77}$$

where I_N is the moment of inertia of the nosewheel landing gear assembly about the steering axis. It should be noted that the acceleration of the airplane was neglected in obtaining Eq. (77).

When the nose wheel is allowed to swivel freely about its steering axis, its skidding angle, β_N, is no longer equal to the airplane's angle of sideslip β; also, Eq. (73) is no longer valid. Therefore, as shown in Figure 16, ξ_N is defined as the effective skidding angle for an unlocked nosewheel, given by

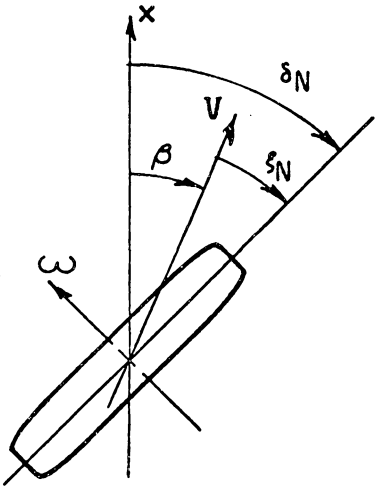

Figure 16. Angular displacement of a freely swiveling nosewheel

$$\xi_N = \delta_N - \beta \quad . \tag{78}$$

Also, let $\bar{\xi}_N$ replace $\bar{\beta}_N$ in Eqs. (68), (69), and (73); thus, the equations of motion for the aircraft with an unlocked nosewheel become

$$\dot{u} = vr - C_1 u^2 - C_2 \tag{79}$$

$$\dot{v} = - ur + C_3 v - C_4 \bar{\beta}_M - C_5 \bar{\xi}_N + C_6 \bar{\beta}_M u^2 + C_7 \bar{\xi}_N u^2 \tag{80}$$

and

$$\dot{r} = C_8 v + C_9 ur + C_{10} \bar{\beta}_M - C_{11} \bar{\xi}_N - C_{12} \bar{\beta}_M u^2 + C_{13} \bar{\xi}_N u^2 + C_{14} \delta_r u^2 \ . \tag{81}$$

Also, Eq. (73) is replaced by the following expression:

$$\bar{\xi}_N = \frac{39}{\mu_{y_N}} \left(\frac{w}{d} \right)_N^2 \xi_N$$

or

$$\bar{\xi}_N = \frac{39}{\mu_{y_N}} \left(\frac{w}{d} \right)_N^2 (\delta_N - \beta) \ . \tag{82}$$

Equations (71), (72), (74) and (75) are valid whether the nosewheel is locked or unlocked.

Hence, the four simultaneous equations (77), (79), (80), and (81) describe the airplane's directional motion during the landing roll if the nosewheel is unlocked. The variables in these equations are u, v, r, and δ_N. However, as discussed previously, it is preferable to solve for the variables β, ψ, $\dot{\psi}$, and δ_N.

(M) Control Considerations.

During the landing roll, after touchdown, some form of control is needed to keep the airplane on the runway. The rudder and the

nosewheel are the usual means of control during the landing ground roll.

If a control analysis of airplane motion during the landing roll is to be performed, a mathematical control equation must be considered in addition to the aircraft equations of motion. This thesis will employ a control function of the form

$$\delta = \delta(e) \tag{83}$$

where δ is the control deflection and e is the error signal to which the control surface is reacting. Equation (83) represents the reaction of the pilot to an abnormal condition; because of its inherent simplicity, this type of closed-loop control function was used instead of a human transfer function. Although it is considered to be of limited value when applied to landing simulations, a closed-loop control function is adequate for the purposes of this thesis.

As an example of Eq. (83), suppose that the nosewheel is used to keep the airplane pointed in the direction of the runway($\psi = 0$). Thus, the nosewheel is used to correct for perturbations in ψ with $\psi = 0$ corresponding to the neutral condition. A simple control function for this situation is

$$\delta_N = -2\psi \quad . \tag{84}$$

An airplane to which Eq. (84) has been applied is shown in Figure 17.

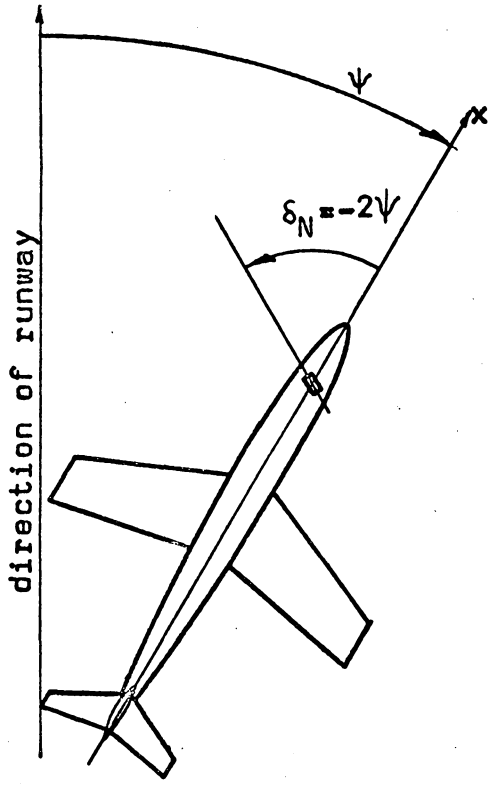

Figure 17. Simple control function

The nosewheel is reacting according to Eq. (84) and is attempting to return the aircraft to its proper direction.

However, the control functions used in this thesis are slightly more complicated than the example given by Eq. (84). The airplane's control mechanism was required to react to perturbations in ψ and $\dot{\psi}$, both of which have neutral points at their zero values. The error signal was given by

$$e = \psi + 4\dot{\psi} \qquad (85)$$

where ψ is in radians and $\dot{\psi}$ is in radians per second.

The control function was similar to the function f(e) shown in Figure 18. For the landing roll simulations performed in this thesis, the function f(e) was represented in the analog computer by a function generator.

The control analysis of the directional motion of the aircraft during the landing roll simulations may be summarized as follows:

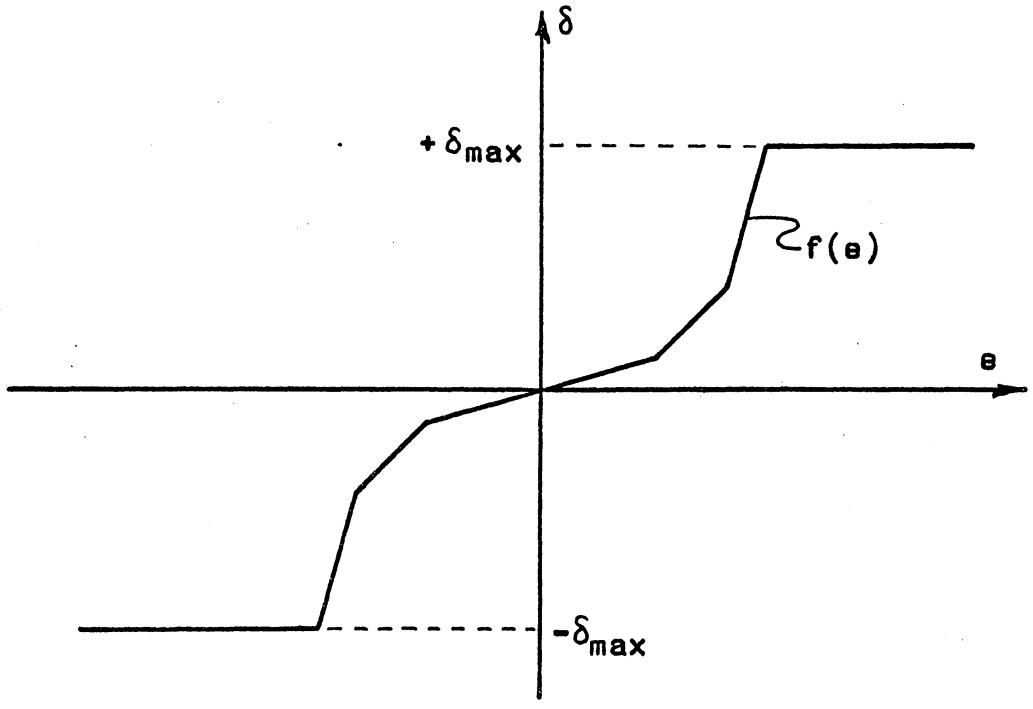

Figure 18. Piecewise continuous control function

(1) When the nosewheel is locked, the rudder is used to control the airplane. For this situation, the motion of the airplane is described by Eqs. (67), (68) and (69) and the control deflections are specified by

$$\delta_r = f(e)$$

where e is given by Eq. (85).

(2) When the nosewheel is unlocked, it is used to steer the airplane. For this situation, the motion of the airplane is described by Eqs. (79), (80) and (81) and the steering

deflection is specified by

$$\delta_N = - f(e)$$

where e is given by Eq. (85).

(N) Application of the Equations of Motion.

If the equations of motion are to be solved they must be applied to a given aircraft. For the purposes of this investigation an airplane model, having the size and characteristics of a supersonic flight-bomber, was selected. Characteristic dimensions and aerodynamic data for this model are noted below:

Dimensions:

$b = 38$ ft

$x_N = 13$ ft

$x_M = 2$ ft

$y_M = 6$ ft

$z = 4$ ft

$S = 400$ ft^2 .

$\epsilon = 0.25$ ft

Mass characteristics:

Landing weight: 18,000 lbs

$I_z = 68{,}000$ slug ft^2

$I_N = 1.8$ slug ft^2 .

Propulsion:

Single engine: T = 10,000 lbs (16,000 lbs with afterburning)

Aerodynamic coefficients:

$C_D = 0.10$

$C_L = 0.8$

$C_{m_{\alpha_L}} = - 0.10$

$C_{m_{\delta_{hs}}} = - 0.78$ per rad

$C_{y_\beta} = - 0.86$ per rad

$C_{n_\beta} = 0.17$ per rad

$C_{n_r} = - 0.27$ sec/rad

$C_{l_\beta} = - 0.14$ per rad

$C_{l_r} = 0.18$ sec/rad

$C_{l_{\delta_a}} = 0.10$ per rad

Control deflections:

horizontal stabilizer: + 0.15 radians (up)
- 0.45 radians (down)

rudder: $\pm$ 0.35 radians

ailerons: $\pm$ 0.25 radians

nosewheel steering: $\pm$ 0.45 radians

Landing gear wheel data:

Main wheels: d = 26 inches

w = 6.6 inches

p = 250 lbs/in^2

Nose wheel: d = 18 inches

w = 5.5 inches

p = 250 lbs/in^2

Other data:

Landing speed: 220 ft/sec

Atmospheric density: $\rho = 2.378 \times 10^{-3}$ slugs/ft^3

The data specified above were used to determine values of the constant coefficients in the landing roll equations. This enabled the solution of the non-linear equations of motion to be obtained on the analog computer. A schematic of the computer circuitry appears in Appendix C. Expressions giving the relation between the potentiometer settings and the constant coefficients is also presented in Appendix C.

It should be noted that the airplane model specified by the above data uses the horizontal tail instead of the elevator for

longitudinal control. This requires the use of the horizontal tail setting, δ_{hs}, instead of the elevator deflection, δ_e, in the equations of motion. The relation between δ_{hs} and α_{hs}, the angle of attack of the horizontal stabilizer, is

$$\delta_{hs} = \alpha_{hs} - \alpha_L \quad .$$

The tailplane setting, δ_{hs}, is measured relative to the fuselage reference line.

VI. DISCUSSION OF RESULTS

Using the analog computer to solve the equations of motion presented in the previous section, a solution for the landing roll path of an airplane on the runway is obtained. An analysis of the airplane's motion during the landing ground roll will give an understanding of the factors which influence the aircraft's motion. In this manner the airplane's directional stability and control during the ground roll can be investigated.

Computer solutions of the equations of motion are depicted in Figures 20 to 30. These figures do not show the motion of the airplane during the entire landing run; i.e., from touchdown to the end of the ground roll. Instead, only that portion of the landing roll which is of primary interest is presented.

For convenience in discussing the results of this study the figures are divided into two groups. The first group consists of Figures 20 through 26, in which the airplane's reactions to a set of non-equilibrium initial conditions are presented. These initial conditions include angles of yaw and sideslip which correspond to an initial sideslipping situation (see Figure 19). The second group consists of Figures 27 through 30, which depict the airplane as initially being in a state of equilibrium and then reacting to a disturbance input at $t = 7$ seconds after the initiation of the

computations. For both groupings an initial forward velocity, other than the touchdown speed, is specified. This initial forward velocity serves simply as a desirable starting point for the computations.

Before actually discussing the results of this investigation some consideration of the airplane's directional stability and control is warranted.

There are two factors to be considered when evaluating the airplane's overall directional stability. First, the contribution of the airplane aerodynamic stability, which is usually stabilizing; and second, the contributions of the airplane's landing gear. The main gear will usually provide a small stabilizing component, while the nosewheel will be highly destabilizing. The rudder has been found to be capable of providing directional control down to speeds of approximately two-thirds the touchdown speed (according to reference 1). However, a different form of control, such as nosewheel steering, is needed to keep the airplane on the runway at lower rolling speeds.

This stability analysis has been conducted with the nosewheel locked in a neutral position, and with all aerodynamic controls fixed. The magnitude of the nosewheel's destabilizing influence is shown in Figure 20 where the relative motion of an airplane, with and without the nosewheel, is presented. The airplane without a nosewheel serves as a mathematical model used to demonstrate the destabilizing

effects of the nosewheel. Although this condition of no nosewheel is not realistic, it can be simulated on a full-scale aircraft by keeping the nosewheel very lightly loaded, or by lifting the nosewheel off the runway slightly.

Without the nosewheel the aircraft exhibits, first, a rapid convergence and then a very mild spiral divergence; this is typical of directional aerodynamic characteristics of airplanes. Conversely, with the nosewheel the airplane is extremely unstable. Thus it appears that the nosewheel has a large destabilizing effect on the airplane during the landing roll.

Figures 21, 22, and 23 show the influence of several of the physical parameters upon the vehicle's motion. In Figure 21, the effect of varying the nosewheel length is presented. It should be noted that, for a tricycle landing gear, the nosewheel length does not materially affect the motion. Also, the distance between the main landing gear wheels will not influence the motion since this parameter does not explicitly appear in the equations of motion.

The airplane which was used as a model for this study employed the horizontal stabilizer, rather than an elevator, as the main means for longitudinal control. An examination of Figure 22 reveals that the effect of the horizontal stabilizer upon the landing roll motion should not be underestimated. When the stabilizer is given a positive angle of attack, it produces a negative pitching moment

which increases the vertical load on the nosewheel. The reverse is true when the horizontal stabilizer is at a negative angle of attack. Hence, Figure 22 indicates that by using the horizontal stabilizer to reduce the load on the nosewheel, the aircraft's landing roll performance is improved. Apparently it is desirable to have the nosewheel loaded as lightly as possible during the landing roll.

In Figure 23, the motion during different portions of the landing roll is presented. This has been accomplished here by varying the initial forward speed, u_o. Thus the airplane's path at different rolling speeds - high, medium, and low - can be evaluated and compared. Although the motion is divergent for all cases, the degree of divergence is greatest at the lowest speeds. This tendency toward greater instability as the speed decreases demonstrates the existence of some residual aerodynamic stability which, as expected, diminishes in effectiveness as speed is reduced. In addition, this reduction in stability is also an indication of the increased destabilizing influence which the nosewheel has at low speeds. It is felt that this is brought about primarily because the coefficient of side friction is largest at low speeds.

From the results of Figures 22 and 23 it can be deduced that, at the higher rolling speeds, the residual aerodynamic stability can be very beneficial, provided that the horizontal stabilizer is used to keep the nosewheel lightly loaded.

The effect of braking on the airplane during the landing roll is demonstrated in Figure 24.

Braking simulations, shown in Figure 24, were obtained under conditions duplicating maximum braking effort. It should be noted that maximum braking has a large degrading influence on the vehicle's stability, and that the airplane's motion diverges quite rapidly. Actually, the divergence shown in Figure 24 is a complete skid. Here, a complete skid is characterized by large values of the angle of sideslip, β. It is reasonable to expect that braking effort less than maximum braking will not cause such a sharp reduction in directional stability during landing roll.

Previously, it had been shown that the longitudinal control (the horizontal stabilizer for this study), if employed properly, can improve the airplane's directional stability during unbraked rolling in landing. Figure 25 illustrates the result of varying the angle of attack of the horizontal tail during maximum braking. It can be seen that the horizontal stabilizer is not as effective in improving the airplane's directional stability during braked rolling as during unbraked rolling. The cause of this reduction in horizontal stabilizer effectiveness may be summarized as follows:

(1) Braking produces a negative pitching moment which increases the load on the nosewheel.

(2) The side forces, produced by the main gear wheels during maximum braking, are much smaller than during unbraked rolling.

(3) During a skidding situation the aerodynamic dihedral effect, C_{ℓ_β}, and the cross derivative, C_{ℓ_r}, combine to produce a rolling moment which loads one of the main wheels more than the other; this, in turn, because of the large values of friction coefficients during braking, produces a significant yawing moment which tends to increase the skid.

The stability analysis discussed previously was conducted with the nosewheel locked. In addition, a stability analysis was performed with the nosewheel free to rotate about its steering axis. Allowing the nosewheel to rotate freely about the steering axis resulted in a stable vehicle motion coupled with an unstable nosewheel oscillation, similar to nosewheel shimmy. The results of this part of this study appeared to be only of academic interest and consequently will not be further elaborated upon.

After the stability analysis was completed a brief investigation on the analog computer was conducted to determine the capabilities of the nosewheel steering as a form of directional control. In summary, the results of this investigation are: it was ascertained that the nosewheel steering provided sufficient control to keep the airplane on the runway for all cases examined. This was true for

both braked and unbraked rolling during the landing run. However, a much greater degree of control, as typified by larger nosewheel steering deflections, was needed to keep the airplane on the runway when subjected to braked rolling.

Only one portion of the nosewheel steering investigation appears to be worthy of mention. This concerns the influence of changes in angle of attack, of the horizontal stabilizer, upon the nosewheel steering. The ability of the nosewheel steering to return the airplane to an equilibrium position, from an initially disturbed condition, is shown in Figure 26 for two different angles of attack of the horizontal stabilizer. With the horizontal tail at its extreme negative angle of attack position, the nosewheel is lightly loaded and the nosewheel steering is able to reduce the angle of yaw, ψ, toward its equilibrium value ($\psi = 0$) from an initial value of ψ_o.

However, with the horizontal tail at an extreme positive angle of attack, the nosewheel is heavily loaded and the steering is unable to effectively reduce the angle of yaw from its initial value, ψ_o. The same control function, which was of the form $\delta_N = - f(\psi)$, was used in both of the above examples. Hence, Figure 26 would seem to indicate that it is better to unload the nosewheel as much as possible during steering; this is contrary to the usual practice of loading the nosewheel as much as possible during steering.

The results of this study would seem to point to one central conclusion - that is, it is best to keep the nosewheel loaded as lightly as possible during the entire landing roll. The computer solutions, presented in Figures 27 through 30, seem to verify this statement.

High-speed rolling is depicted in Figures 27 and 28. During the high-speed roll the nosewheel is locked, as is usually done to prevent nosewheel shimmy, and directional control is provided by the rudder. The airplane is initially pointed straight down the center of the runway; and a disturbance is encountered at t = 7 seconds. The aircraft is easily controlled with a lightly loaded nosewheel; but, with a heavily loaded nosewheel, and the same amount of control, it is difficult to control the aircraft. Eventually it veers off the runway, although not actually entering into a full skid.

Figures 29 and 30 present the low-speed case, under the same set of circumstances, except that nosewheel steering is used to control the aircraft. Once again, the airplane is most easily controlled when the nosewheel is lightly loaded rather than when it is heavily loaded.

To complete this study, several investigations were undertaken to determine the effects of adverse weather conditions - wet and icy runways - on the landing roll of the aircraft. These adverse weather situations resulted in slightly improved performance with the

nosewheel locked; but, there was no difference between dry and slippery surfaces when nosewheel steering was used to control the aircraft. It should be pointed out that these results must be viewed as inconclusive; particularly in view of the limitations imposed by the assumptions made. The limitations, are essentially that the wheel's rolling motion is maintained (no slip occurs) on these slippery surfaces despite the reduced friction coefficients. To remove these limitations would involve a study of wheel dynamics and of the frictional properties of slippery surfaces; such a study is beyond the scope of this thesis.

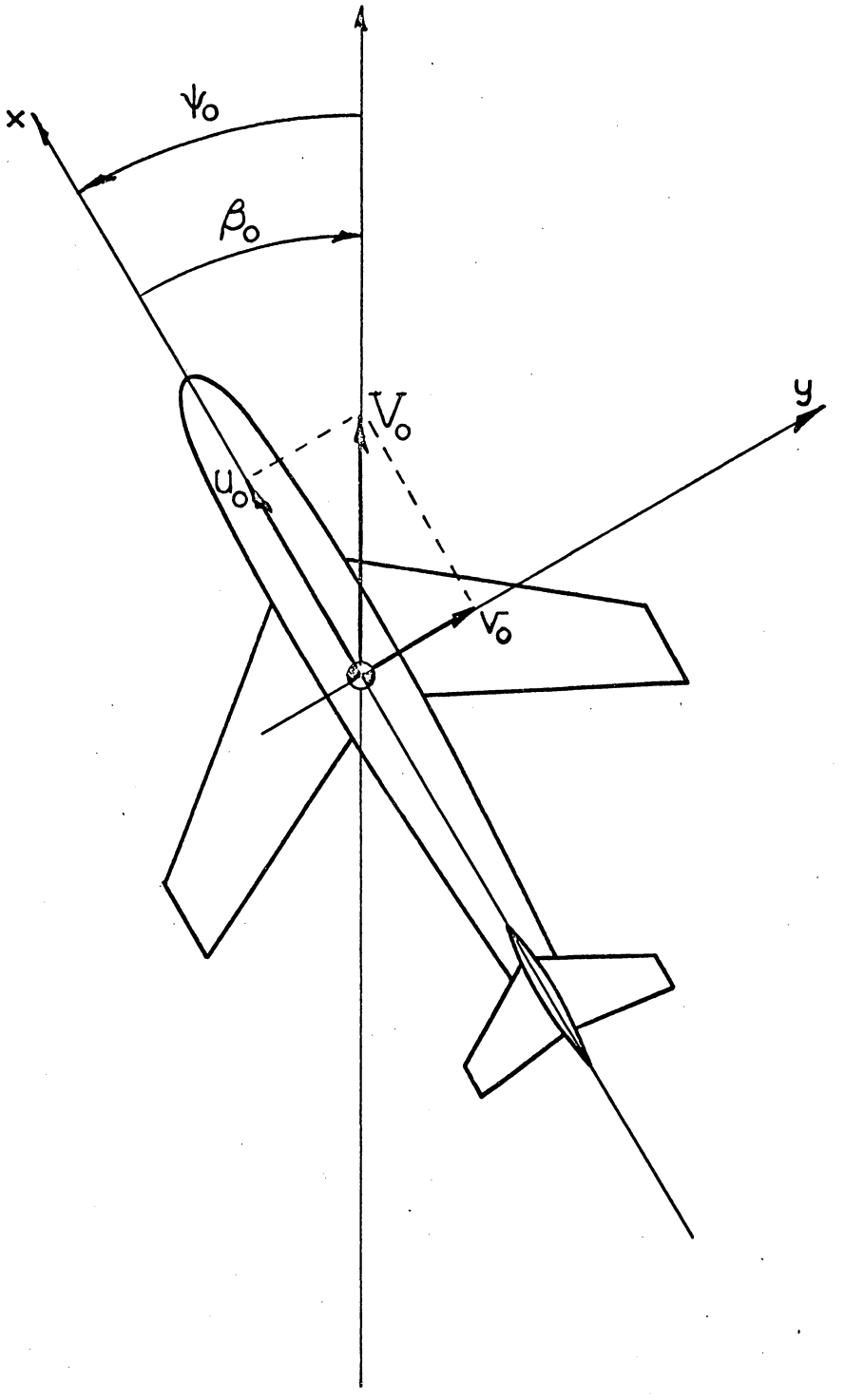

Figure 19. Initial Conditions

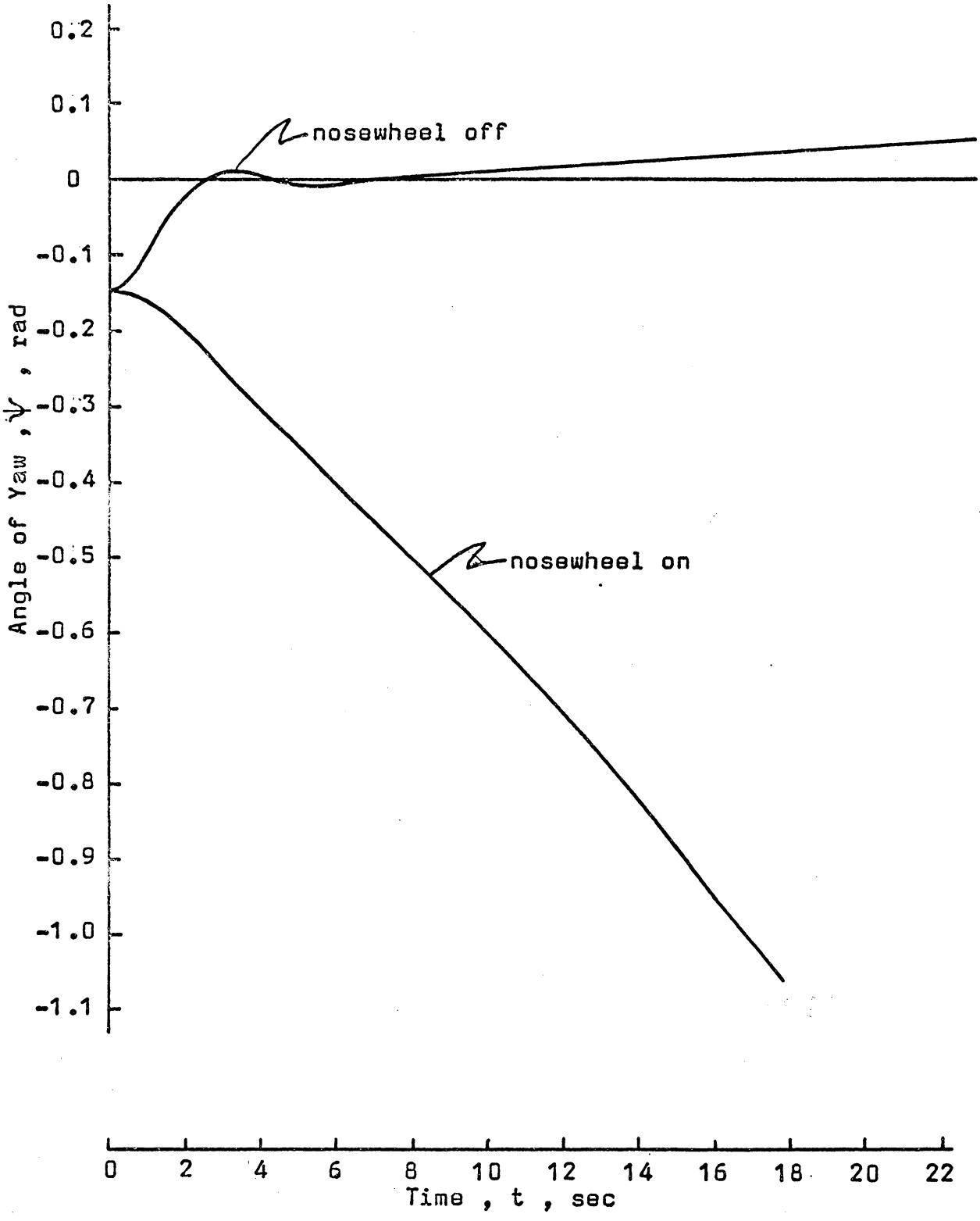

Figure 20a. Directional stability contribution of the nosewheel during the landing roll

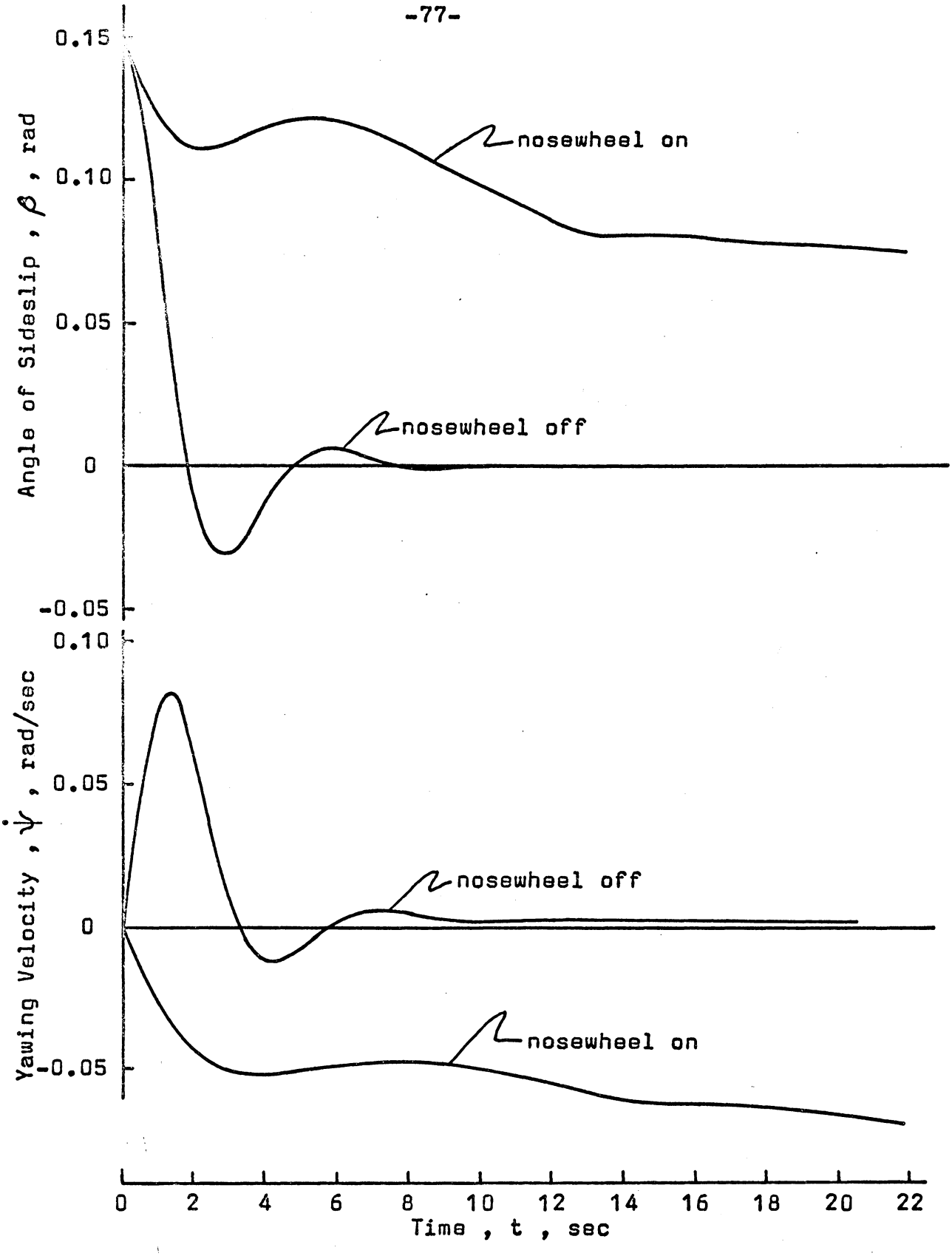

Figure 20b. Directional stability contribution of the nose-wheel during the landing roll

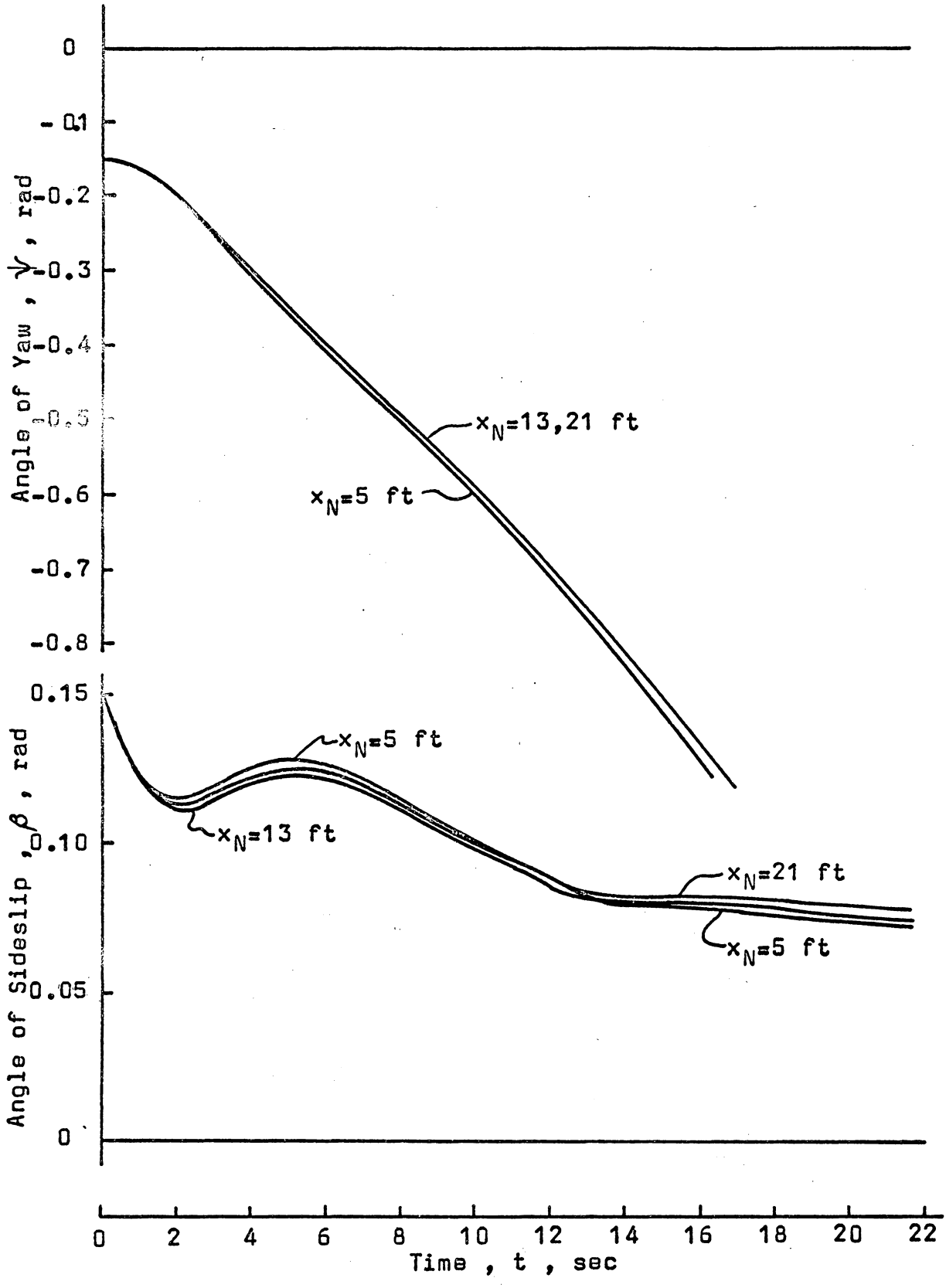

Figure 21. The effect of varying the nosewheel length on an airplane's motion during the landing roll

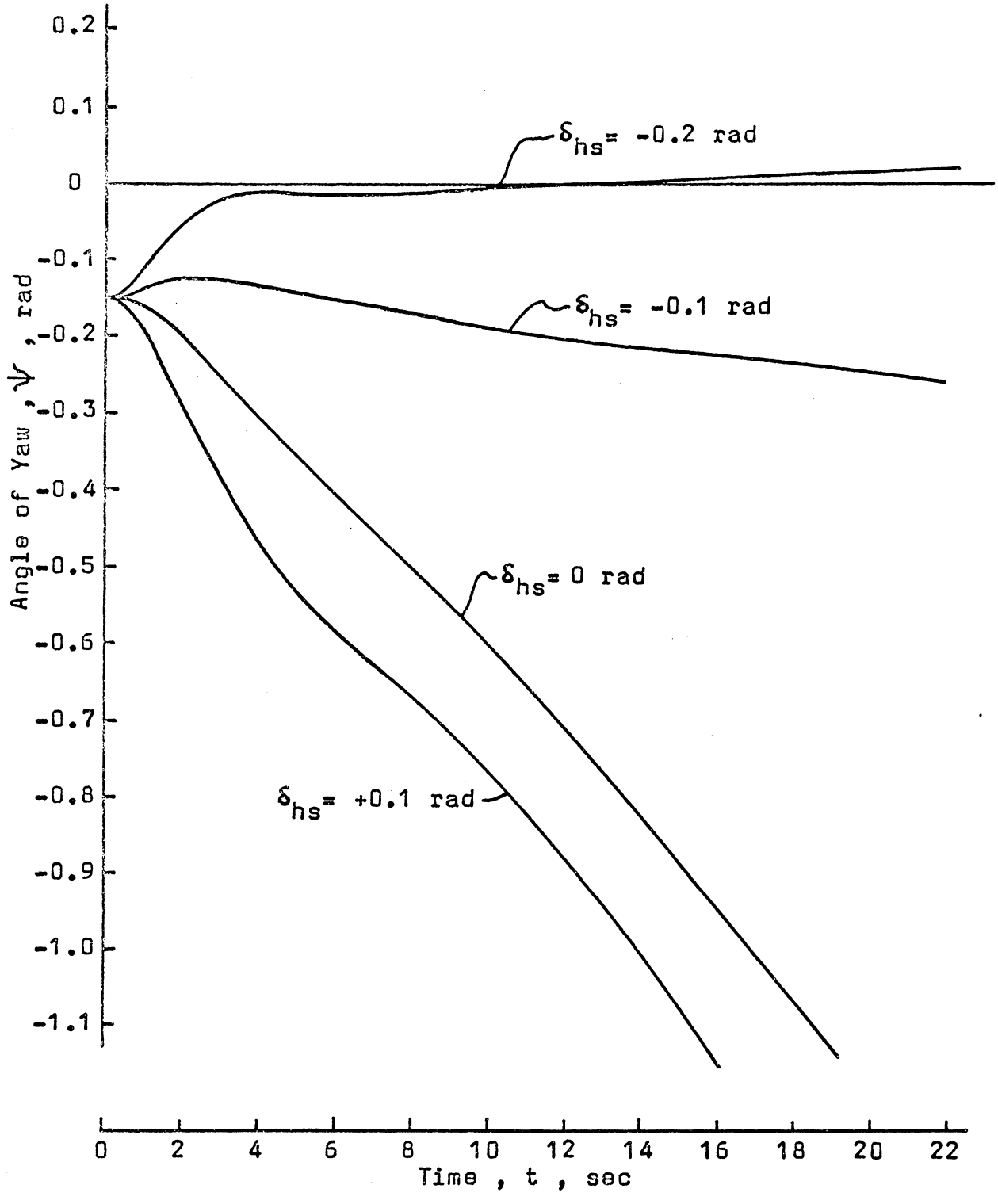

Figure 22a. The influence of horizontal stabilizer incidence on an airplane's motion during the landing roll

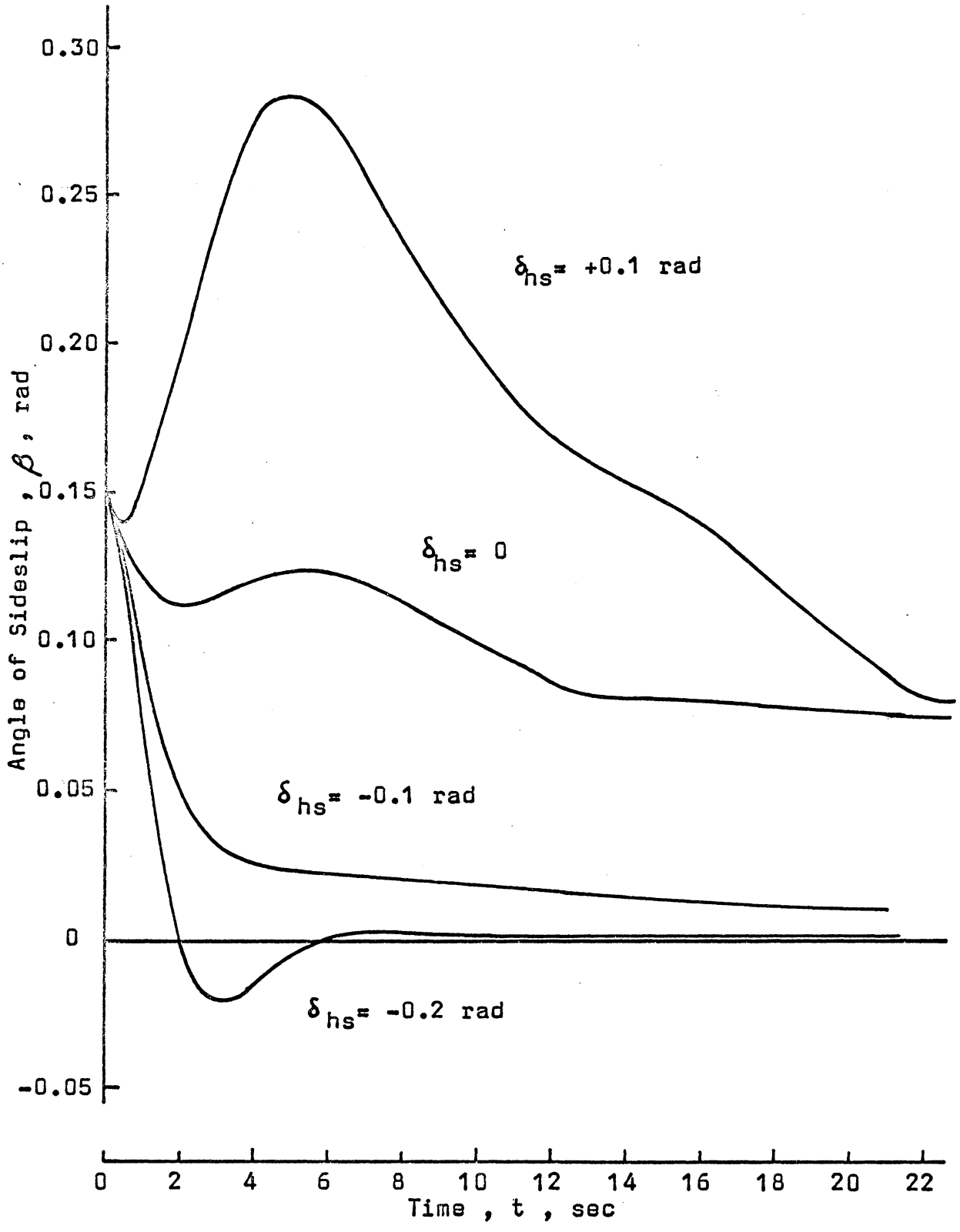

Figure 22b. The influence of horizontal stabilizer incidence on an airplane's motion during the landing roll

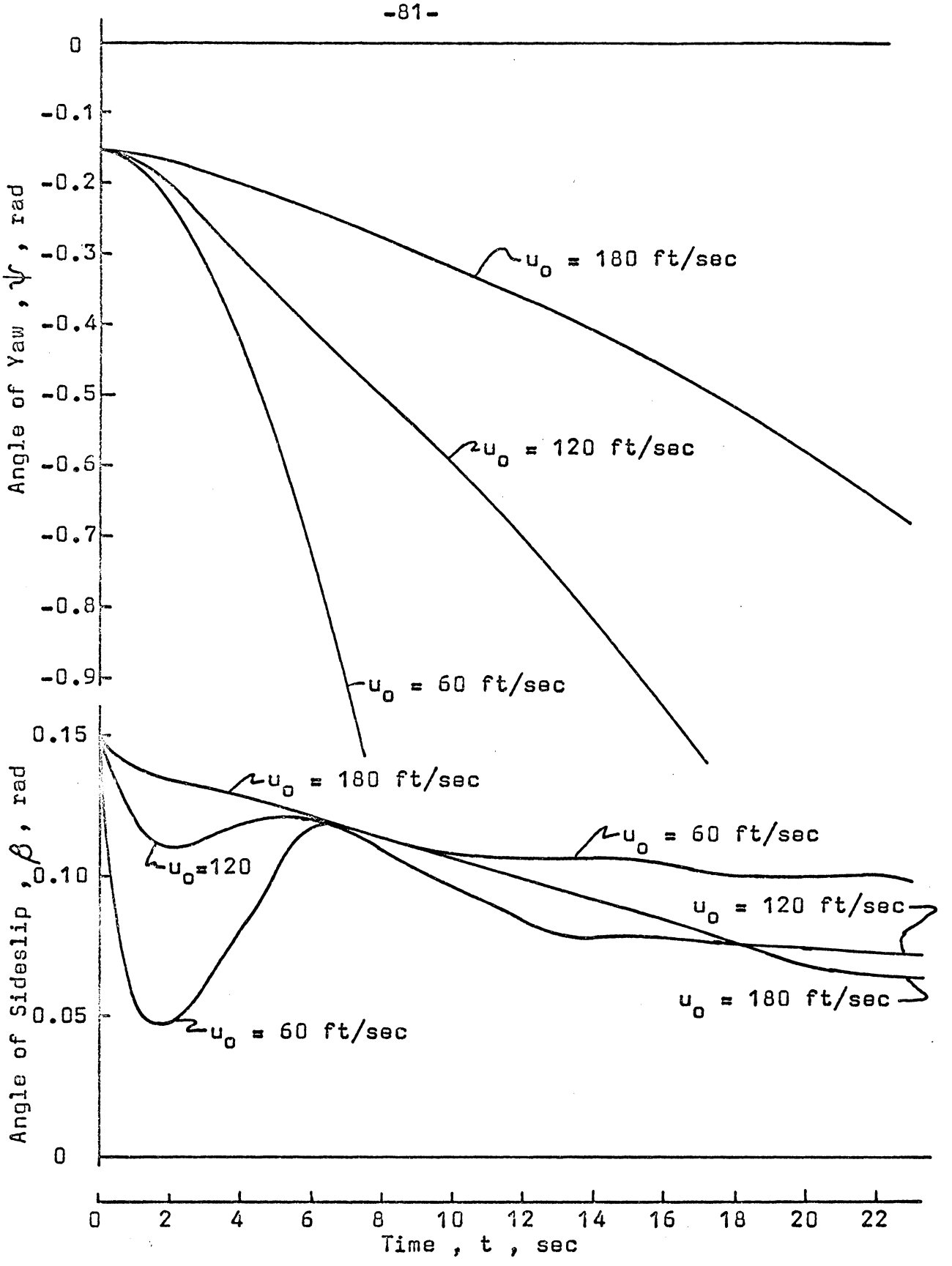

Figure 23. The effect of changing the initial forward speed condition upon an airplane's motion during the landing roll

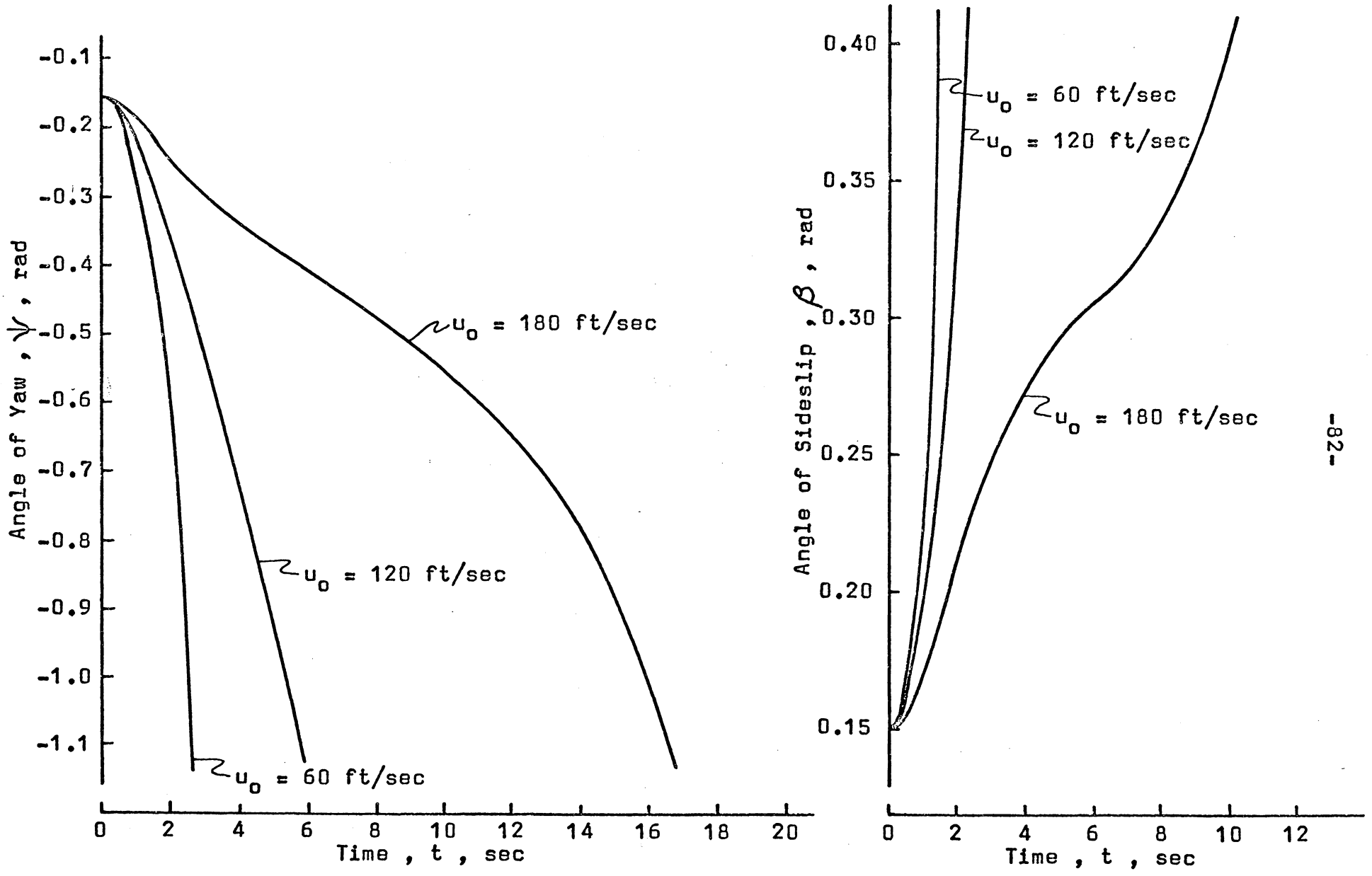

Figure 24. The motion of an aircraft subject to braking during the landing roll

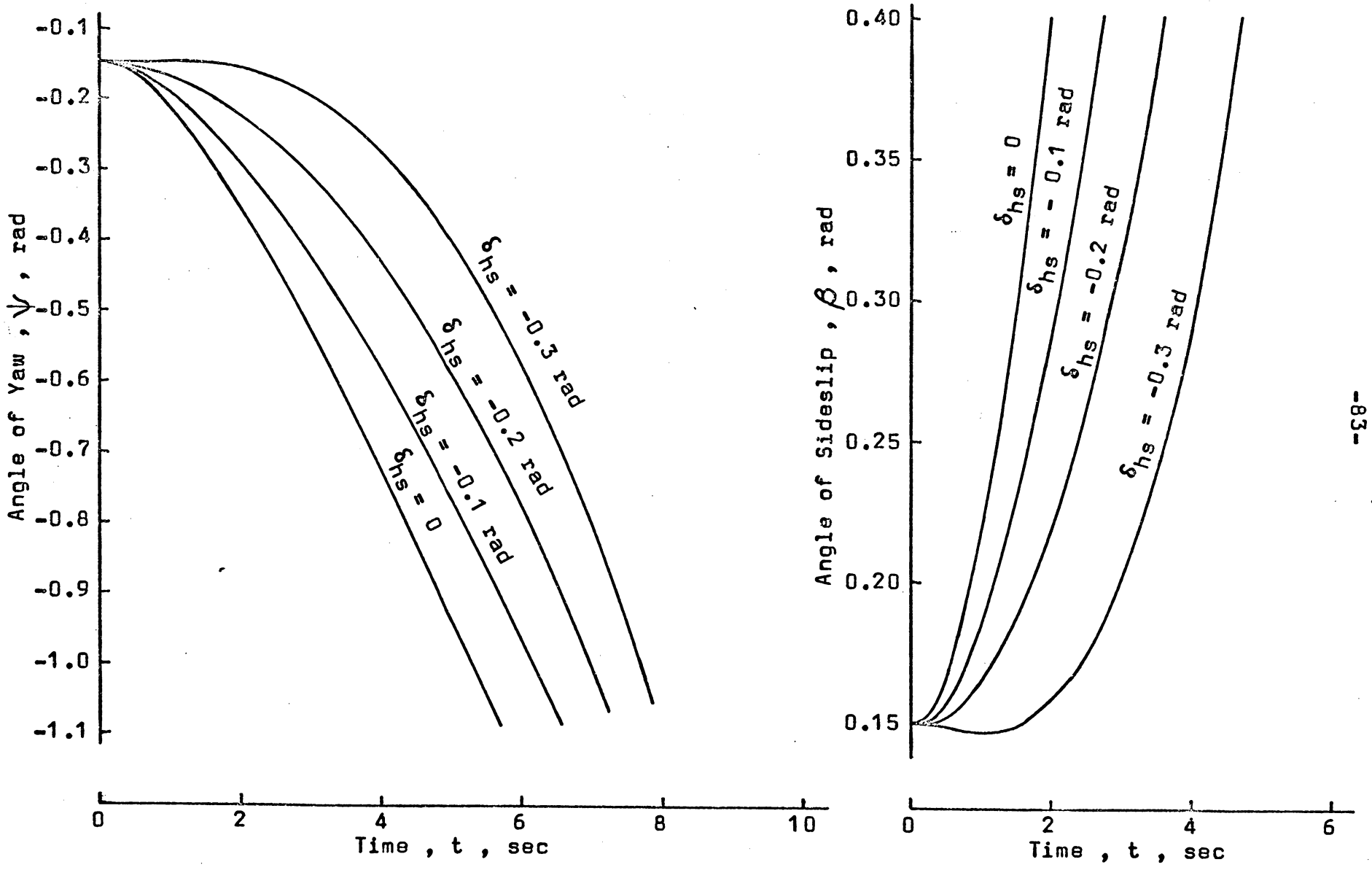

Figure 25. The influence of horizontal stabilizer incidence on the motion of an aircraft subject to braking

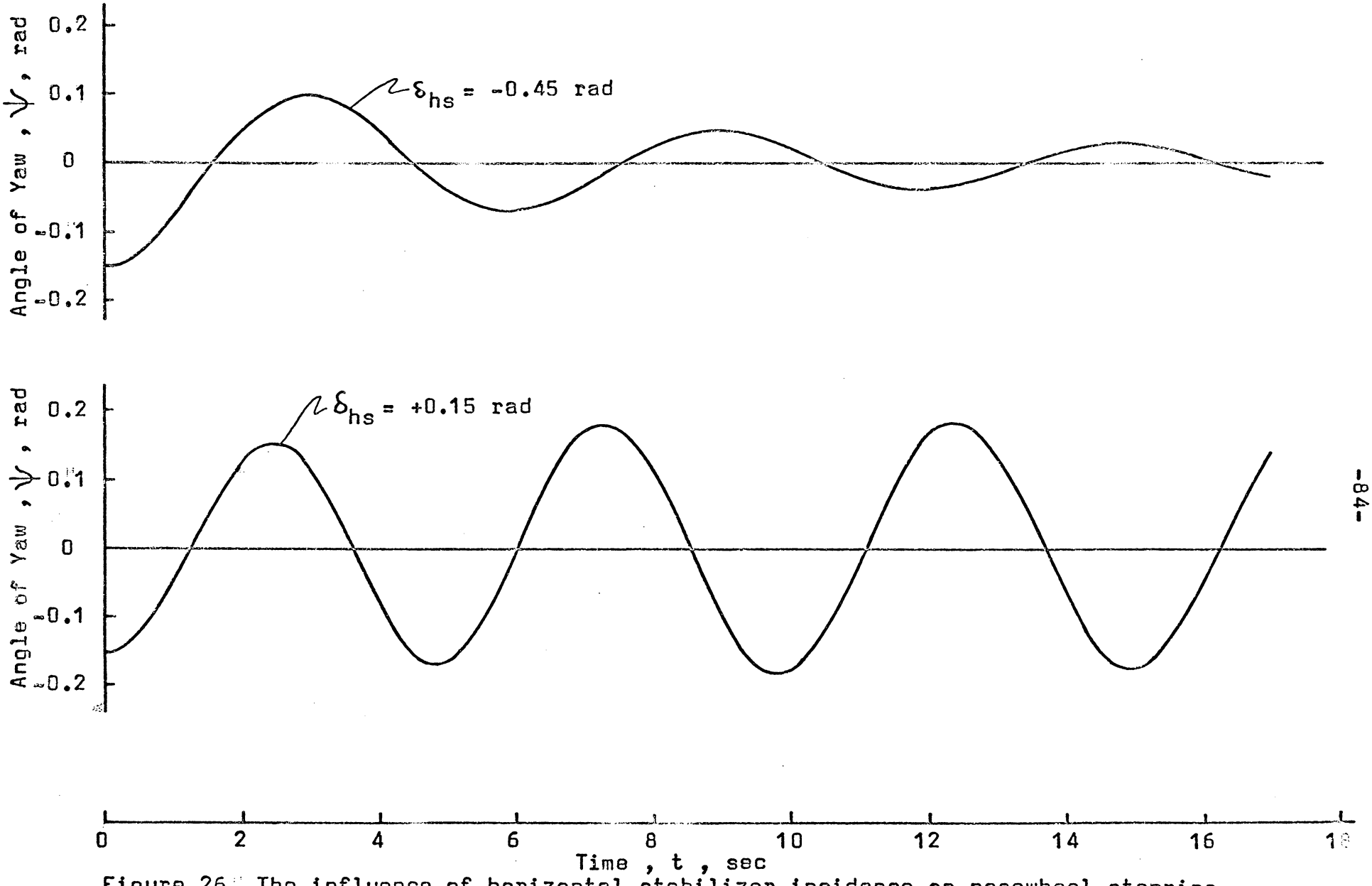

Figure 26. The influence of horizontal stabilizer incidence on nosewheel steering during the landing roll

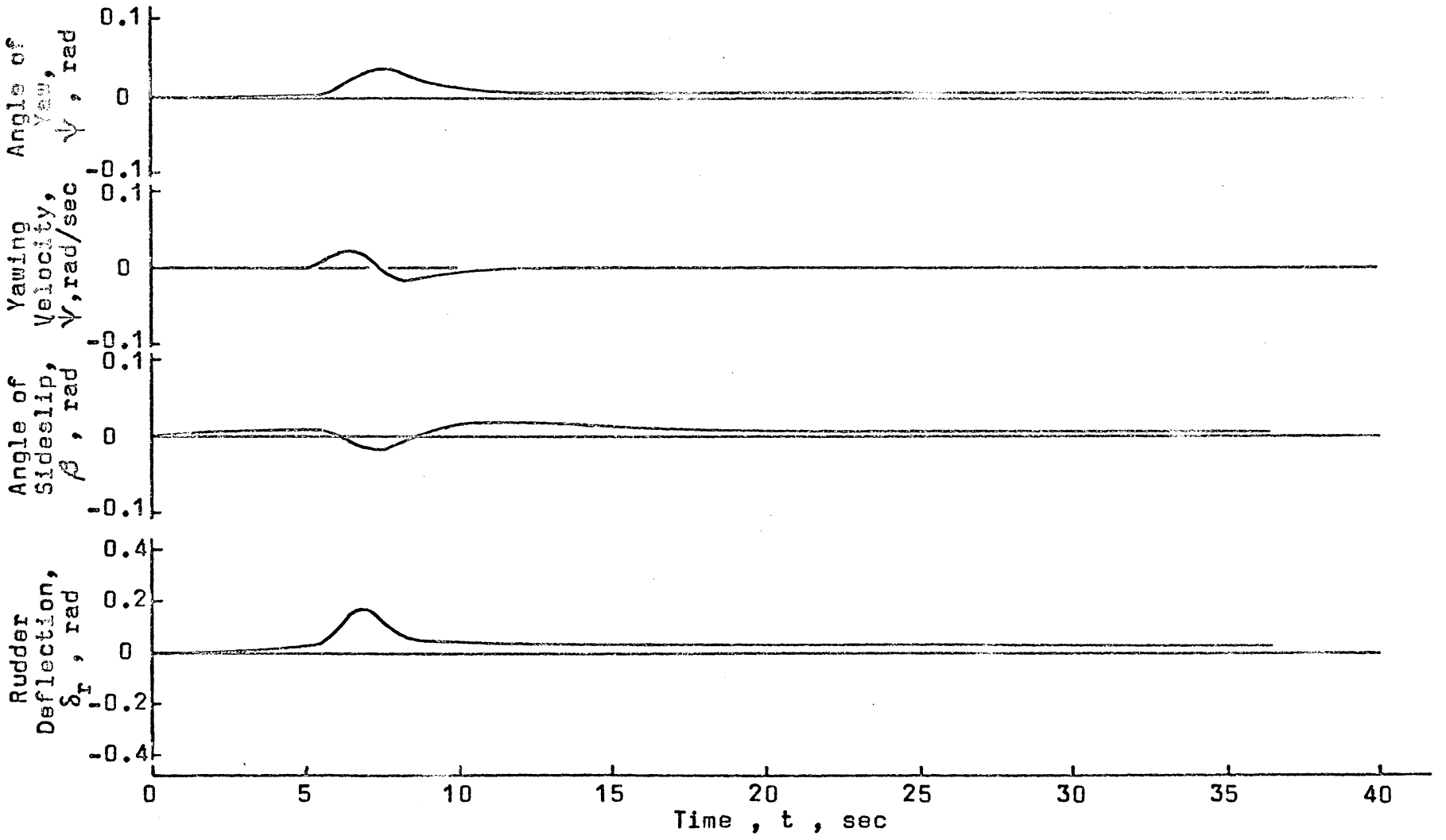

Figure 27. Motion of an aircraft at high rolling speeds with the nosewheel locked and lightly loaded

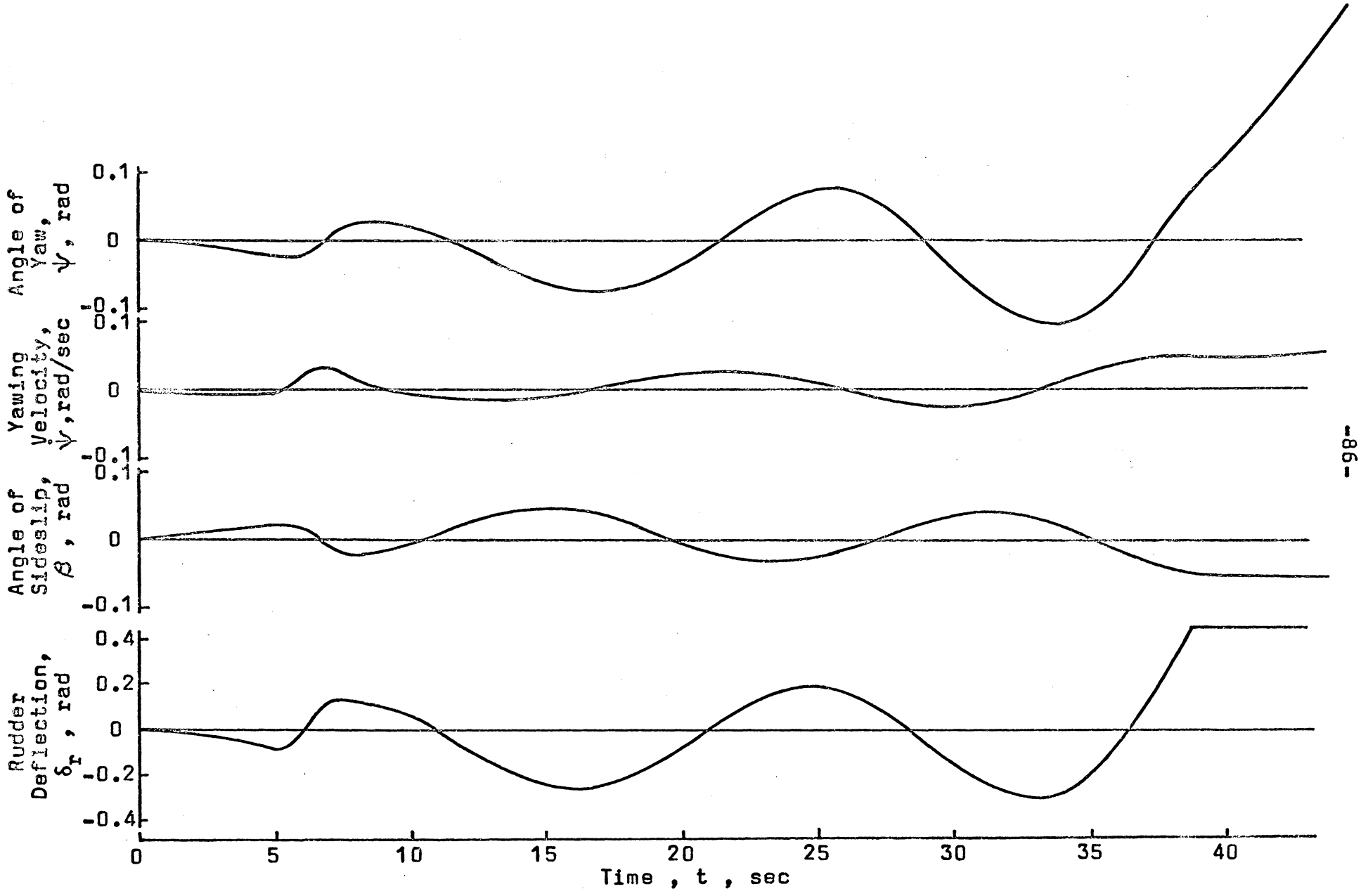

Figure 28. Motion of an aircraft at high rolling speeds with the nosewheel locked and heavily loaded

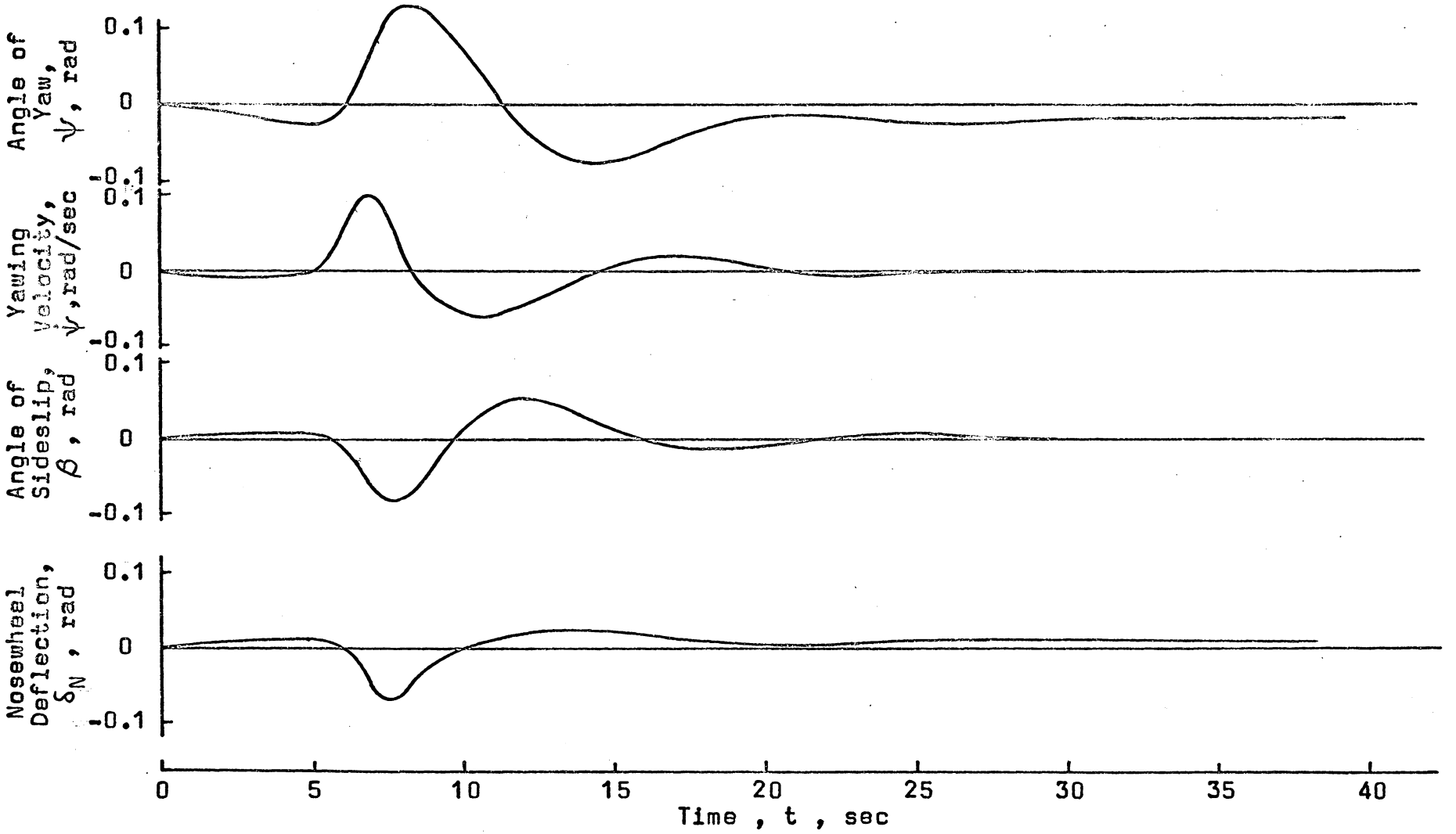

Figure 29. Motion of an aircraft at low rolling speeds with the nosewheel unlocked and lightly loaded

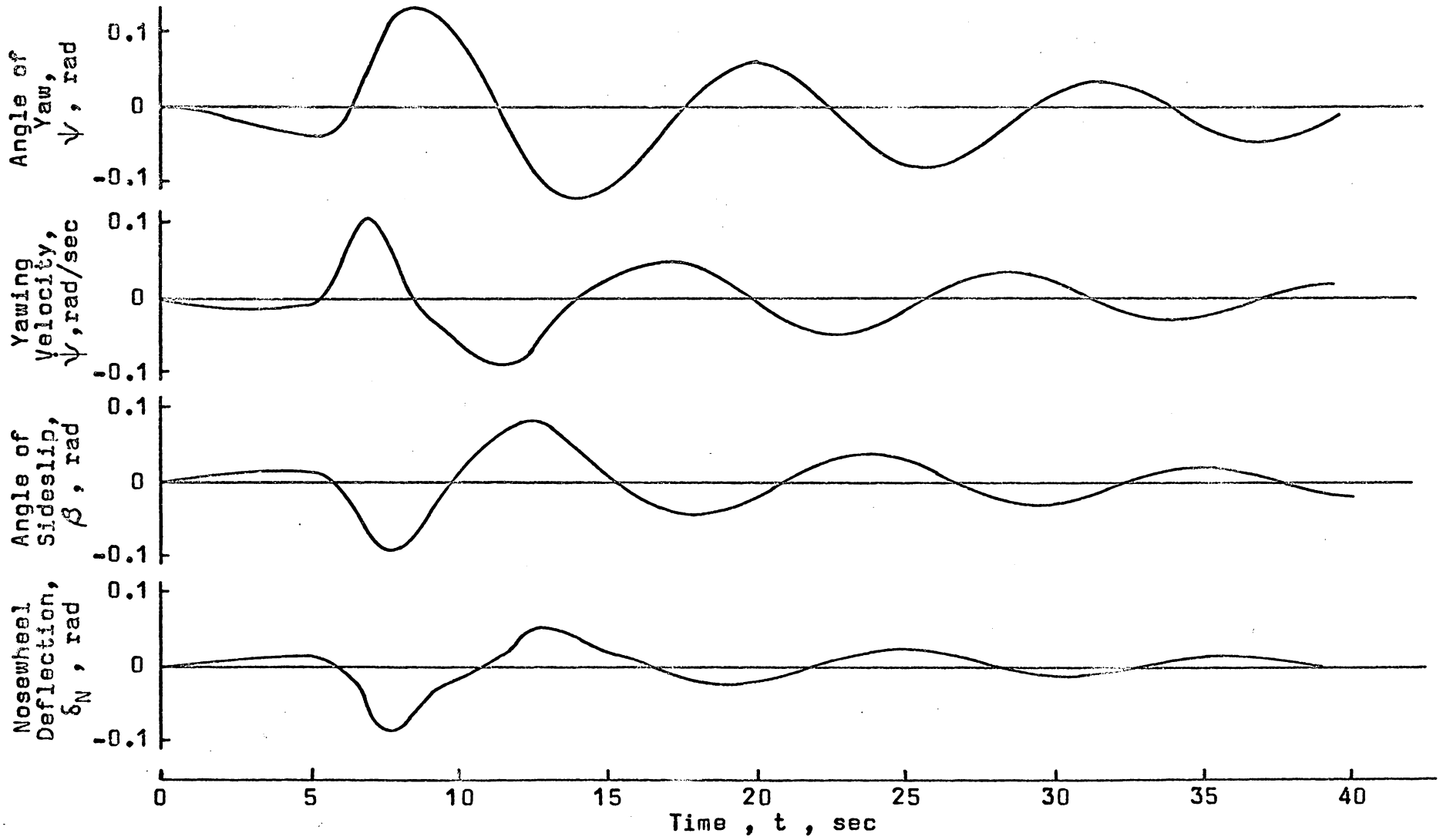

Figure 30. Motion of an aircraft at low rolling speeds with the nosewheel unlocked and heavily loaded

VII. CONCLUSIONS

In view of the results obtained in this study the following general conclusions, regarding the directional dynamics of an aircraft during the landing ground roll, have been developed:

(1) The nosewheel presents a large destabilizing influence on the overall directional stability during the landing roll. This destabilizing influence can be greatly reduced if the longitudinal control (horizontal stabilizer or elevator) is used to keep the nosewheel lightly loaded.

(2) Evidentally there is no reason to believe that difficulties with the directional motion of the aircraft during the landing run will be encountered under normal operating conditions. The directional controls available to the pilot are normally powerful enough to keep the airplane on the runway during its landing roll. However, it is possible that serious trouble can develop, due to pilot error or incorrect manipulation of the controls. These could possibly lead to overcontrol and, then, to situations which the pilot cannot overcome.

(3) If serious trouble does occur during the early phases of landing roll, the first step toward countering the difficulty

should be to reduce the vertical load on the nosewheel as much as possible. However, the chances of encountering difficulties will be minimized if the load on the nosewheel is maintained at a small level for as long as possible during the landing roll.

(4) If trouble does develop during the braking phase of rolling, the brakes should be released, since braked rolling is a highly unstable condition. Also, recovery from dangerous situations would be easier under the conditions of free, or unbraked, rolling.

(5) The landing ground roll problem should be separated into two speed regimes - the high-speed regime, where there is enough residual aerodynamics to influence the motion and where aerodynamic control is employed; and, the low speed regime, where the aerodynamic forces are negligible and where nosewheel steering is needed to give directional control to the aircraft. The boundary between these two regimes may be defined as the speed at which the elevator or horizontal stabilizer is no longer able to lift the nosewheel off the ground.

(6) The high-speed regime is basically the less troublesome since there is some residual aerodynamic stability, and because the elevator or horizontal stabilizer is capable of countering

the undesirable characteristics of a locked nosewheel. Conversely, the high-speed regime can be very troublesome if the elevator or horizontal stabilizer is used to increase the load on the nosewheel.

(7) There does not appear to be any satisfactory changes which can be made to the basic design of tricycle landing gear to improve the handling qualities of an airplane during the landing roll.

VIII. ACKNOWLEDGMENTS

The author would like to express his gratitude to Dr. James B. Eades, Jr., for his assistance in conducting this investigation and for his patience in the preparation of this thesis.

IX. REFERENCES

1. Thomas, J. W. H.: TAKEOFF AND LANDING PROBLEMS - DESIGN FOR RUNWAY CONDITIONS. Journal of the Royal Aeronautical Society, Vol. 67, No. 633, September 1963, pp 571-576.

2. Smiley, Robert F. and Horne, Walter B.: MECHANICAL PROPERTIES OF PNEUMATIC TIRES WITH SPECIAL REFERENCE TO MODERN AIRCRAFT TIRES. NASA TR R-64, 1960.

3. Pike, E. C.: COEFFICIENTS OF FRICTION. Journal of the Royal Aeronautical Society, Volume 56, No. 466, December 1949, pp 1085-1094.

4. Horne, Walter B. and Dreher, Robert C.: PHENOMENA OF PNEUMATIC TIRE HYDROPLANING. NASA TN D-2056, November 1963.

5. Bourcier de Carbon, Christian: ANALYTICAL STUDY OF SHIMMY OF AIRPLANE WHEELS. NACA TM 1337, September 1962.

X. BIBLIOGRAPHY

1. Greenwood, Donald T.: PRINCIPLES OF DYNAMICS. Prentice Hall, Englewood Cliffs, New Jersey, 1965, pp 362-366.

2. Harrin, Eziaslav N.: LOW TIRE FRICTION AND CORNERING FORCES ON A WET SURFACE. NACA TN 4406, Sept. 1958.

3. Horne, Walter B.; Stephenson, Bertrand H.; and Smiley, Robert F.: LOW-SPEED YAWED ROLLING AND SOME OTHER ELASTIC CHARACTERISTICS OF TWO 56-INCH-DIAMETER, 24-PLY-RATING AIRCRAFT TIRES. NACA TN 3235, August 1954.

4. Horne, Walter B.; Smiley, Robert F.; and Stephenson, Bertrand H.: LOW-SPEED YAWED ROLLING CHARACTERISTICS AND OTHER ELASTIC PROPERTIES OF A PAIR OF 26-INCH-DIAMETER, 12-PLY-RATING, TYPE VII AIRCRAFT TIRES. NACA TN 3604, May 1956.

5. Horne, Walter B.; and Smiley, Robert F.: LOW SPEED YAWED ROLLING CHARACTERISTICS AND OTHER ELASTIC PROPERTIES OF A PAIR OF 40-INCH-DIAMETER, 14-PLY-RATING, TYPE VII AIRCRAFT TIRES. NACA TN 4109, January 1958.

6. Horne, Walter B. and Leland, Trafford J. W.: INFLUENCE OF TIRE TREAD PATTERN AND RUNWAY SURFACE CONDITION ON BRAKING FRICTION AND ROLLING RESISTANCE OF A MODERN AIRCRAFT TIRE. NASA TN D-1376, September 1962.

7. Jackson, Charles T., Jr., and Snyder, C. Thomas: VALIDATION OF A RESEARCH SIMULATOR FOR INVESTIGATING JET TRANSPORT HANDLING QUALITIES AND AIRWORTHINESS CRITERIA DURING TAKEOFF. NASA TN D-3565, October 1966.

8. James, M. L.; Smith, G. M.; and Wolford, J. C.: ANALOG AND DIGITAL COMPUTER METHODS IN ENGINEERING ANALYSIS. International Textbook Co., Scranton, Pennsylvania, 1964, pp 1-198.

9. Perkins, Courtland D. and Hage, Robert E.: AIRPLANE PERFORMANCE, STABILITY, AND CONTROL. John Wiley and Sons, New York, 1949, pp. 315-338 and 374-470.

10. Rhody, Francis J.: RUNWAY TRACTION. Proceedings of the American Society of Civil Engineers, Journal of the Aero-Space Transport Division, Vol. 92, No. AT 2, October 1965, pp. 51-56.

11. Sawyer, Richard H. and Kolnick, Joseph J.: TIRE-TO-SURFACE FRICTION COEFFICIENT MEASUREMENTS WITH A C-123B AIRPLANE ON VARIOUS RUNWAY SURFACES. NASA TR R-20, 1959.

12. Seckel, Edward: STABILITY AND CONTROL OF AIRPLANES AND HELICOPTERS. Academic Press, New York, 1964, pp. 218-250 and 422-427.

The vita has been removed from the scanned document

XII. APPENDICES

APPENDIX A

Derivation of the Equations of Motion with Respect to a System of Body Axes

Translational Equations.

Newton's equation, in vector form, is

$$\vec{F} = m\,\vec{a} = m\,\dot{\vec{V}} \tag{A-1}$$

where this equation is written with respect to an inertial axis system and for a constant mass. However, when considered relative to a body axis system (x, y, z) the force, $\vec{F}$, and the velocity, $\vec{V}$, are written as

$$\vec{F} = F_x\,\vec{e}_x + F_y\,\vec{e}_y + F_z\,\vec{e}_z \tag{A-2}$$

and

$$\vec{V} = u\,\vec{e}_x + v\,\vec{e}_y + w\,\vec{e}_z \quad . \tag{A-3}$$

To obtain the absolute acceleration, $\vec{a}$ or $\dot{\vec{V}}$, with respect to the body axes, the following differentiation formula is used:

$$\dot{\vec{V}} = \frac{d\vec{V}}{dt} = \left(\frac{d\vec{V}}{dt}\right)_{\text{relative}} + \vec{\omega} \times \vec{V} \tag{A-4}$$

Where

$$\left(\frac{d\vec{V}}{dt}\right)_{\text{relative}} = \dot{u}\,\vec{e}_x + \dot{v}\,\vec{e}_y + \dot{w}\,\vec{e}_z \tag{A-5}$$

and

$$\vec{\omega} = p\,\vec{e}_x + q\,\vec{e}_y + r\,\vec{e}_z \quad . \tag{A-6}$$

Hence, by combining Eqs. (A-1) through (A-6), Newton's equation, relative to a set of body axes, is obtained as

$$F_x \vec{e}_x + F_y \vec{e}_y + F_z \vec{e}_z = m\left[(\dot{u} + wq - vr) \vec{e}_x + (\dot{v} + ur - wp) \vec{e}_y + (\dot{w} + vp - uq) \vec{e}_z \right] . \quad \text{(A-7)}$$

Thus, the three scalar translational equations of motion are:

$$\sum F_x = m(\dot{u} + wq - vr) \quad \text{(A-8)}$$

$$\sum F_y = m(\dot{v} + ur - wp) \quad \text{(A-9)}$$

$$\sum F_z = m(\dot{w} + vp - uq) \quad \text{(A-10)}$$

Rotational Equations.

The rotational equation of motion is

$$\vec{M} = \dot{\vec{H}} \quad \text{(A-11)}$$

where $\vec{M}$ is the externally applied moment, and $\vec{H}$ is the angular momentum referred to the center of gravity. Relative to a set of body axes, these quantities become

$$\vec{M} = L \vec{e}_x + M \vec{e}_y + N \vec{e}_z \quad \text{(A-12)}$$

and

$$\vec{H} = h_x \vec{e}_x + h_y \vec{e}_y + h_z \vec{e}_z . \quad \text{(A-13)}$$

Now, as in the previous case

$$\vec{M} = \dot{\vec{H}} = \left(\frac{d\vec{H}}{dt} \right)_{\text{relative}} + \vec{\omega} \times \vec{H} \quad \text{(A-14)}$$

where

$$\left(\frac{d\vec{H}}{dt}\right)_{relative} = \dot{h}_x \vec{e}_x + \dot{h}_y \vec{e}_y + \dot{h}_z \vec{e}_z \quad . \tag{A-15}$$

Note that the moments of inertia and the products of inertia are considered to be constants. So, by combining Eqs. (A-12) through (A-15), the rotational equation of motion becomes:

$$L \vec{e}_x + M \vec{e}_y + N \vec{e}_z = (\dot{h}_x + h_z q - h_y r) \vec{e}_x +$$

$$(\dot{h}_y + h_x r - h_z p) \vec{e}_y + (\dot{h}_z + h_y p - h_x q) \vec{e}_z \quad . \tag{A-16}$$

The expressions for h_x, h_y, and h_z are:

$$h_x = I_x p - I_{xy} q - I_{xz} r \tag{A-17}$$

$$h_y = I_y q - I_{yx} p - I_{yz} r \tag{A-18}$$

and

$$h_z = I_z r - I_{zx} p - I_{zy} q \quad , \tag{A-19}$$

but, if it is assumed that the xz-plane is a plane of symmetry, or that the y-axis is a principal axis, which is the usual case for an airplane, then

$$I_{xy} = I_{yx} = I_{yz} = I_{zy} = 0 \quad .$$

Hence, the expressions for h_x, h_y, and h_z reduce to:

$$h_x = I_x p - I_{xz} r \tag{A-20}$$

$$h_y = I_y q \tag{A-21}$$

and

$$h_z = I_z r - I_{zx} p \quad . \tag{A-22}$$

Now, substituting the above expressions into Equation (A-16), the rotational equation of motion for an airplane is:

$$\begin{aligned} L\,\hat{e}_x + M\,\hat{e}_y + N\,\hat{e}_z = &\left[I_x \dot{p} - I_{xz} \dot{r} + (I_z - I_y)\, qr - I_{xz}\, pq \right] \hat{e}_x + \\ &\left[I_y \dot{q} + (I_x - I_z)\, rp + I_{xz}\, (p^2 - r^2) \right] \hat{e}_y + \\ &\left[I_z \dot{r} - I_{xz} \dot{p} + (I_y - I_x)\, pq + I_{xz}\, qr \right] \hat{e}_z \quad . \end{aligned} \tag{A-23}$$

The three scalar rotational equations of motion for an airplane are:

$$\sum L = I_x \dot{p} - I_{xz} \dot{r} + (I_z - I_y)\, qr - I_{xz}\, pq \tag{A-24}$$

$$\sum M = I_y \dot{q} + (I_x - I_z)\, rp + I_{xz}\, (p^2 - r^2) \tag{A-25}$$

and

$$\sum N = I_z \dot{r} - I_{xz} \dot{p} + (I_y - I_x)\, pq + I_{xz}\, qr \quad . \tag{A-26}$$

APPENDIX B

Derivation of an Empirical Formula for the Value of the Coefficient of Rolling Friction for a Yawed Tire

An attempt was made to develop an empirical relation which would give the variation of the in-plane force acting on a wheel as the yaw-angle of the wheel was increased. Data applying to several type VII aircraft tires was obtained from NACA Technical Notes 3235, 3604, and 4109.

These data, contained in these publications, appeared to be of doubtful accuracy, especially at large yaw angles. However, the accuracy appeared good enough to give a reasonably approximate expression for the coefficient of rolling friction. The principle problem here was that the original tests, or experiments, were concerned primarily with measuring the side force acting on a yawed wheel. Hence, the drag force was measured to an accuracy of only $\pm$ 300 pounds while the side force was measured to an accuracy of $\pm$ 3 pounds. Since the drag force constituted the major portion of the in-plane force, a large scatter resulted when these data were plotted.

The tests were conducted on dry concrete surfaces and for a wide range of tire pressures and loadings. An examination of these

data showed that an empirical formula could not be developed readily to cover the entire range of pressures and loadings. Therefore, it was decided to limit this investigation to the pressures and loadings for which the tires were designed, and at which they were intended to be used under average operating conditions. To satisfy this requirement, the ratio

$$\frac{p\ R_{rat}}{p_{rat}\ R}$$

was selected. Subsequent analysis of the data showed that in order to obtain a reasonable empirical relation, the useful range of this ratio should be limited to

$$0.7 \leqslant \frac{p\ R_{rat}}{p_{rat}\ R} \leqslant 1.4 \quad .$$

For values of the above ratio within the given range, the coefficient of rolling friction, or

$$\mu_r = \frac{F_x}{R} \quad , \qquad \text{(B-1)}$$

was plotted against the yaw angle. These plots showed that as β was increased, μ_r increased to a peak value, and then decreased to zero as shown in Figure B-1. Hence, in order to find a single curve which would match all of the data, it was decided to examine the values of $\mu_{r_{max}}$ and β_{max}.

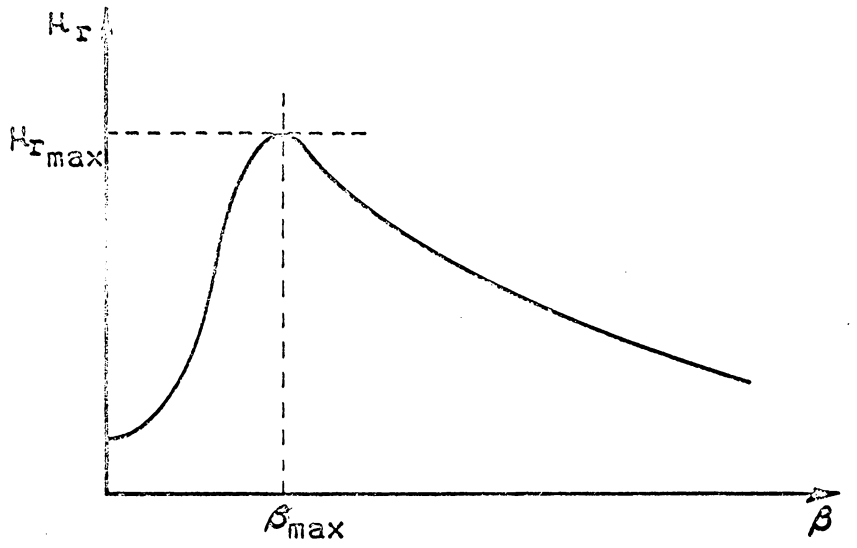

Figure B-1

A subsequent analysis of $\mu_{r_{max}}$ showed that the value of $\mu_{r_{max}}$ is a function of the ratio

$$\frac{p\, R_{rat}}{p_{rat}\, R} \left(\frac{d}{w} \right)^2 \quad .$$

Note that since $A \approx \frac{R}{p}$ and $A_{rat} \approx \frac{R_{rat}}{p_{rat}}$, the above ratio indicates that μ_r is primarily a function of the tire footprint area, A. The tire footprint area, A, is not exactly equal to $\frac{R}{p}$ because of the tire carcass stiffness. The non-dimensional ratio $\left(\frac{d}{w} \right)^2$ appears to take care of the effects of this stiffness in the ratio.

The term β_{max} was found to be a function of the non-dimensional ratio

$$\frac{dw}{R} (p + p_{rat})$$

or

$$\frac{p}{R} \left(1 + \frac{p_{rat}}{p}\right) dw \quad .$$

Thus, for values of $\frac{p\,R_{rat}}{p_{rat}\,R}$, in the range from 0.7 to 1.4, the coefficient of rolling friction can be reasonably predicted by the empirical equation

$$\theta = 0.03 + \frac{\lambda^2}{25}(19 - 14\lambda) \quad \text{for} \quad 0 \leq \lambda \leq 1.0$$

$$\theta = \frac{1}{2300}(8\lambda - 31)^2 \quad \text{for} \quad 1.0 \leq \lambda \leq \frac{31}{8} \qquad \text{(B-2)}$$

$$\theta = 0 \quad \text{for} \quad \lambda \geq \frac{31}{8}$$

where $$\theta = \frac{p\,R_{rat}}{p_{rat}\,R}\left(\frac{d}{w}\right)^2 \mu_r \qquad \text{(B-3)}$$

and $$\lambda = \frac{dw}{R}(p + p_{rat})\,\beta \qquad \text{(B-4)}$$

(β is in radians) .

Equation (B-2) is plotted, in Figure (B-2), with experimental values from NACA Technical Notes 3235, 3604, and 4109.

Note that for values of λ greater than 3.875, the coefficient of rolling friction is zero. This is not exactly the case, but for all practical purposes μ_r is negligible about this value.

Equation (B-2) applies only for low forward speeds. Data which would permit a satisfactory extension of Equation (B-2) to high speed

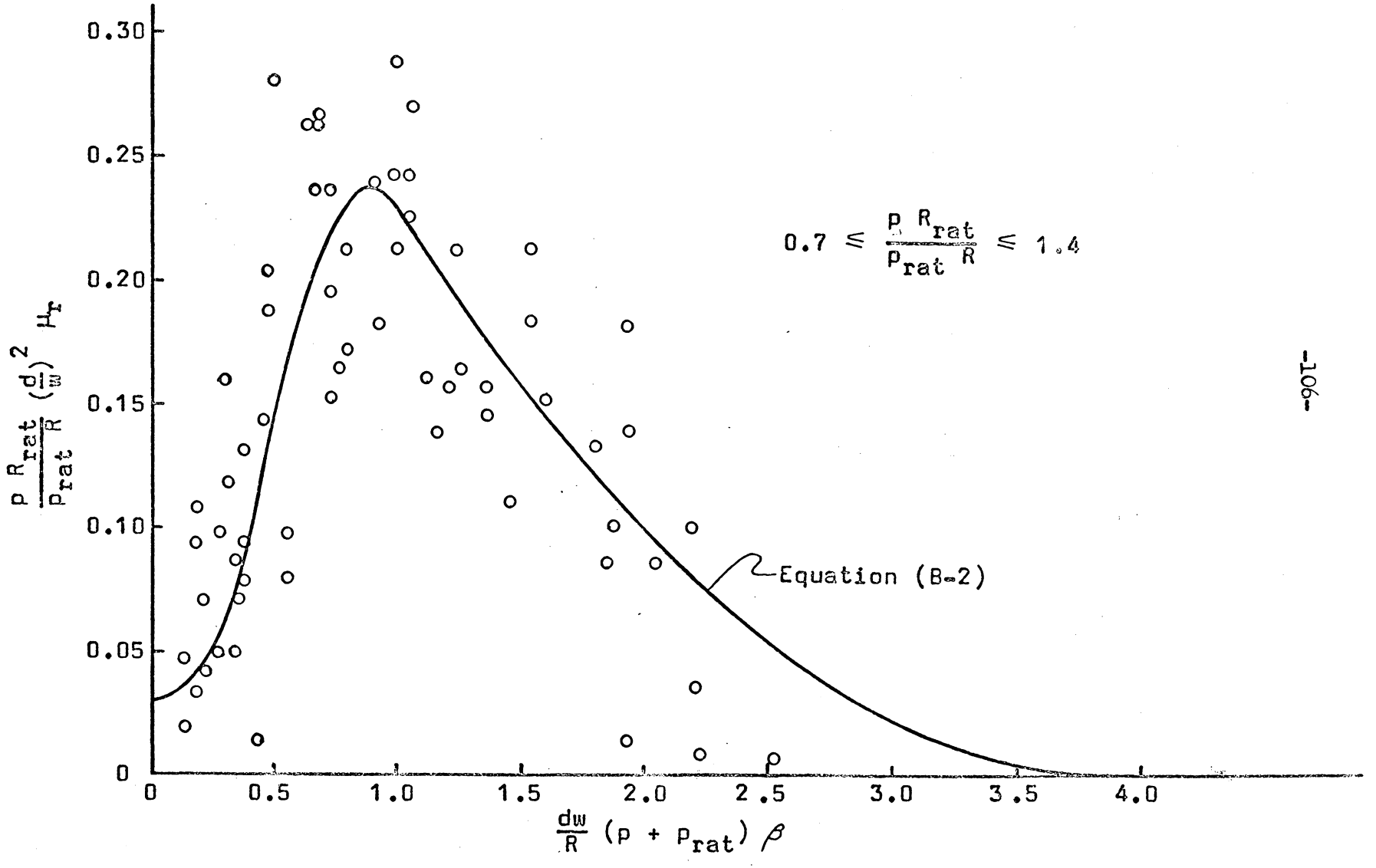
0.30
0.25
0.20
0.15
0.10
0.05
0
0
0.5
1.0
1.5
2.0
2.5
3.0
3.5
4.0
$\frac{p\,R_{rat}}{p_{rat}\,R}\left(\frac{d}{w}\right)^2 \mu_r$
$\frac{dw}{R}(p + p_{rat})\,\beta$
$0.7 \leq \frac{p\,R_{rat}}{p_{rat}\,R} \leq 1.4$
Equation (B-2)

Figure B-2

rolling was not available. However, NASA Technical Note D-1376, NACA TN 4406, and Reference 3 suggest that by letting

$$\theta = \theta' = \frac{400 \quad p\, R_{rat}}{p_{rat}\, R(V + 400)} \left(\frac{d}{w} \right)^2 \mu_r \qquad \text{(B-5)}$$

$$\lambda = \lambda' = \frac{40\, dw\, (p + p_{rat})}{R\, (V + 40)} \beta \qquad \text{(B-6)}$$

where V is in feet/second, Equation (B-2) would be reasonably accurate at higher rolling speeds for small values of β.

Hence

$$\theta' = 0.03 + \frac{\lambda'^2}{25} (19 - 14\, \lambda') \quad \text{for } 0 \leq \lambda' \leq 1.0$$

$$\theta' = \frac{1}{2300} (8\, \lambda' - 31)^2 \quad \text{for } 1.0 \leq \lambda' \leq \frac{31}{8} \qquad \text{(B-7)}$$

$$\theta' = 0 \quad \text{for} \quad \lambda' \geq \frac{31}{8} \; .$$

APPENDIX C

Computer Schematic

Because the landing roll equations of motion are non-linear, an analytic solution of these equations is difficult to obtain. Thus, in the interest of obtaining a quick solution, the landing roll equations of motion are solved on an analog computer.

Summarizing, the landing roll equations for an airplane with nosewheel steering are of the form:

$$u = \int_o^t (v\dot{\psi} - C_1 u^2 - C_2)\, dt + u_o \tag{C-1}$$

$$v = \int_o^t (-u\dot{\psi} + C_3 v - C_4 \bar{\beta}_M - C_5 \bar{\xi}_N + C_6 \bar{\beta}_M u^2 + C_7 \bar{\xi}_N u^2)\, dt + v_o \tag{C-2}$$

$$\dot{\psi} = \int_o^t (C_8 v + C_9 u\dot{\psi} + C_{10} \bar{\beta}_M - C_{11} \bar{\xi}_N - C_{12} \bar{\beta}_M u^2 + C_{13} \bar{\xi}_N u^2)\, dt + \dot{\psi}_o \tag{C-3}$$

$$\psi = \int_o^t \dot{\psi}\, dt + \psi_o \tag{C-4}$$

$$\bar{\beta}_M = \frac{39}{\mu_y} \left(\frac{w}{d} \right)_M^2 \beta \quad ; \quad -1 \leq \bar{\beta}_M \leq +1 \tag{C-5}$$

$$\bar{\xi}_N = \frac{39}{\mu_y} \left(\frac{w}{d} \right)_N^2 \xi_N \quad ; \quad -1 \leq \bar{\xi}_N \leq +1 \tag{C-6}$$

$$\xi_N = \delta_N - \beta \tag{C-7}$$

$$\delta_N = f(e) \tag{C-8}$$

and

$$e = \psi + 4\dot{\psi} \quad . \tag{C-9}$$

The function f(e) given in Eq. (C-8) is presented in Figure (C-1) in terms of the computer voltages. It should be noted that if the nosewheel is locked, $\delta_N = 0$ and $\bar{\beta}_N$ replaces $\bar{\xi}_N$ in Eqs. (C-1) through (C-9).

The computer circuitry required to solve the above equations is shown in Figure (C-2). An explanation of the symbols used is presented in Figure (C-3). These two figures are self-explanatory except for the dotted connection which is noted "unlocked nosewheel" . The circuit is drawn for an airplane which has a clocked nosewheel. If the nosewheel is unlocked and used to steer the aircraft, the input to potentiometer number 17 is replaced by the dotted connection marked "unlocked nosewheel" .

The scale-factor relation between the electronic voltages used by the computer and the physical variables is given in Table C-1, and the coefficient potentiometers settings can be obtained from the expressions given in Table C-2.

Table C-1

variable	electronic voltage	scale-factor relation
u(f/s)	e_1	$e_1 = 0.5\ u$
v(f/s)	e_2	$e_2 = 2.0\ v$
$\dot{\psi}$(rad/sec)	e_3	$e_3 = 200\ \dot{\psi}$
ψ(rad)	e_4	$e_4 = 50\ \psi$
$\bar{\beta}_N$	e_5	$e_5 = 55\ \bar{\beta}_N$ [1]
$\bar{\beta}_M$	e_6	$e_6 = 55\ \bar{\beta}_M$ [1]
β(rad)	e_7	$e_7 = 50\ \frac{e_2}{e_1} = 200\ \beta$
δ_N(rad)	e_8	$e_8 = 200\ \delta_N$
ξ_N(rad)	e_9	$e_9 = 200\ \xi_N$

Notes:

1. This scale-factor is decided by the value of the zener or limiting voltage of 55 volts which is made to correspond to the limiting values of $\bar{\beta}_M$ and $\bar{\beta}_N$.

2. No relation appears for the error voltage e_{10} because the error signal e is defined for convenience and it has no physical significance.

Table C-2

Potentiometer	Potentiometer Setting
1	$2.0 \times 10^{3}\ C_1$
2	$5.0 \times 10^{-2}\ C_2$
3	$3.636\ C_{10}$
4	$-1.455 \times 10^{5}\ C_{13}$
5	$3.636\ C_{11}$
6	$1.455 \times 10^{5}\ C_{12}$
7	$-2.0 \times 10^{1}\ C_9$
8	$1.0 \times 10^{2}\ C_8$
9	$-5.0\ C_3$
10	$1.455 \times 10^{3}\ C_6$
11	$3.636 \times 10^{-2}\ C_4$
12	$-7.273 \times 10^{3}\ C_7$
13	$3.636 \times 10^{-1}\ C_5$
14	$5.0 \times 10^{-3}\ u_o$
15	$2.0 \times 10^{-2}\ v_o$
16	$-5.0 \times 10^{-1}\ \psi_o$
17	$1.0725 \frac{1}{\mu_{y_N}} \left(\frac{w}{d}\right)^2_N$
18	$1.0725 \frac{1}{\mu_{y_M}} \left(\frac{w}{d}\right)^2_N$

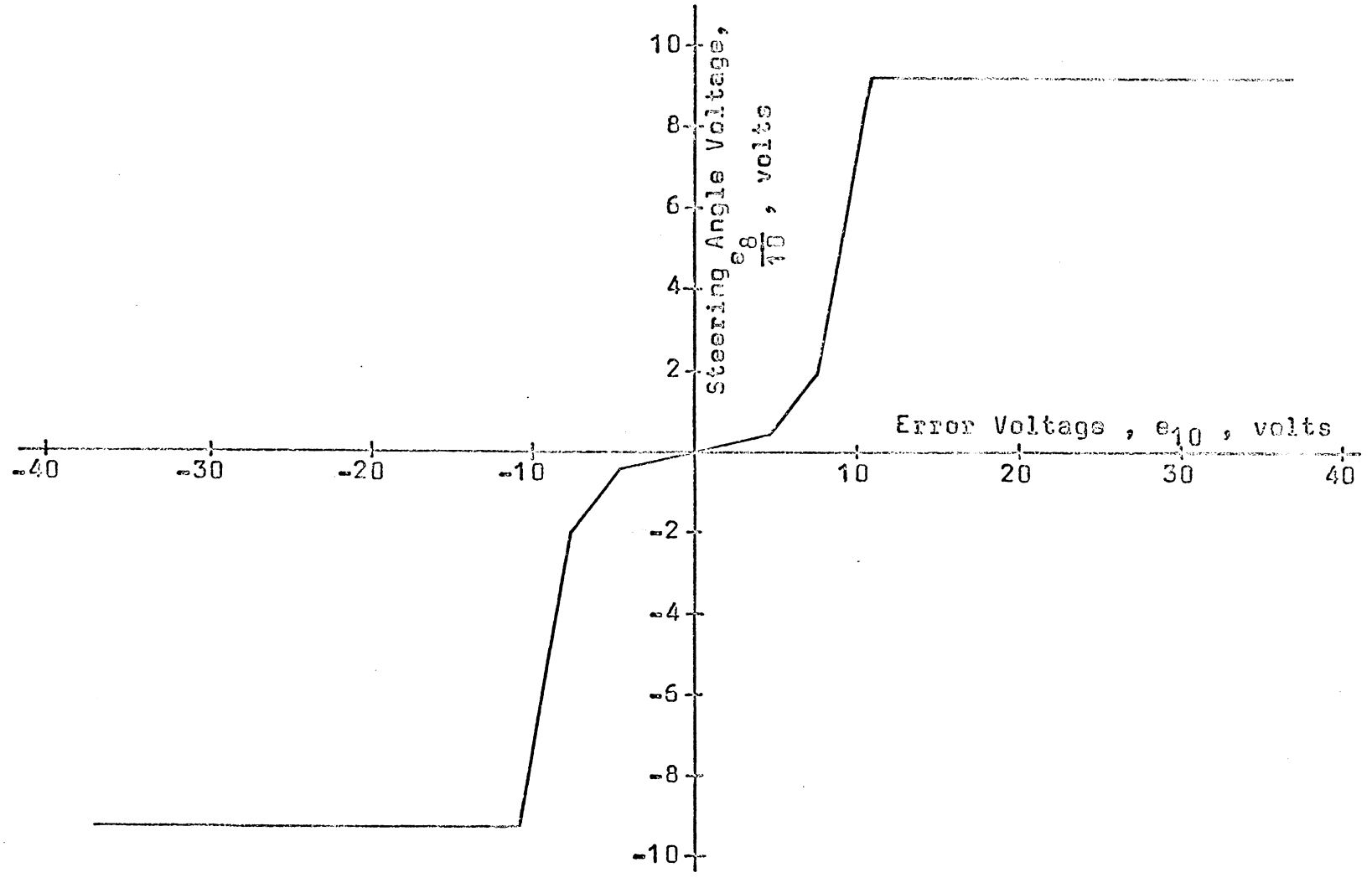
Steering Angle Voltage, $e_{\frac{8}{10}}$, volts
Error Voltage, e_{10}, volts
10
8
6
4
2
-2
-4
-6
-8
-10
-40
-30
-20
-10
10
20
30
40

Figure C-1

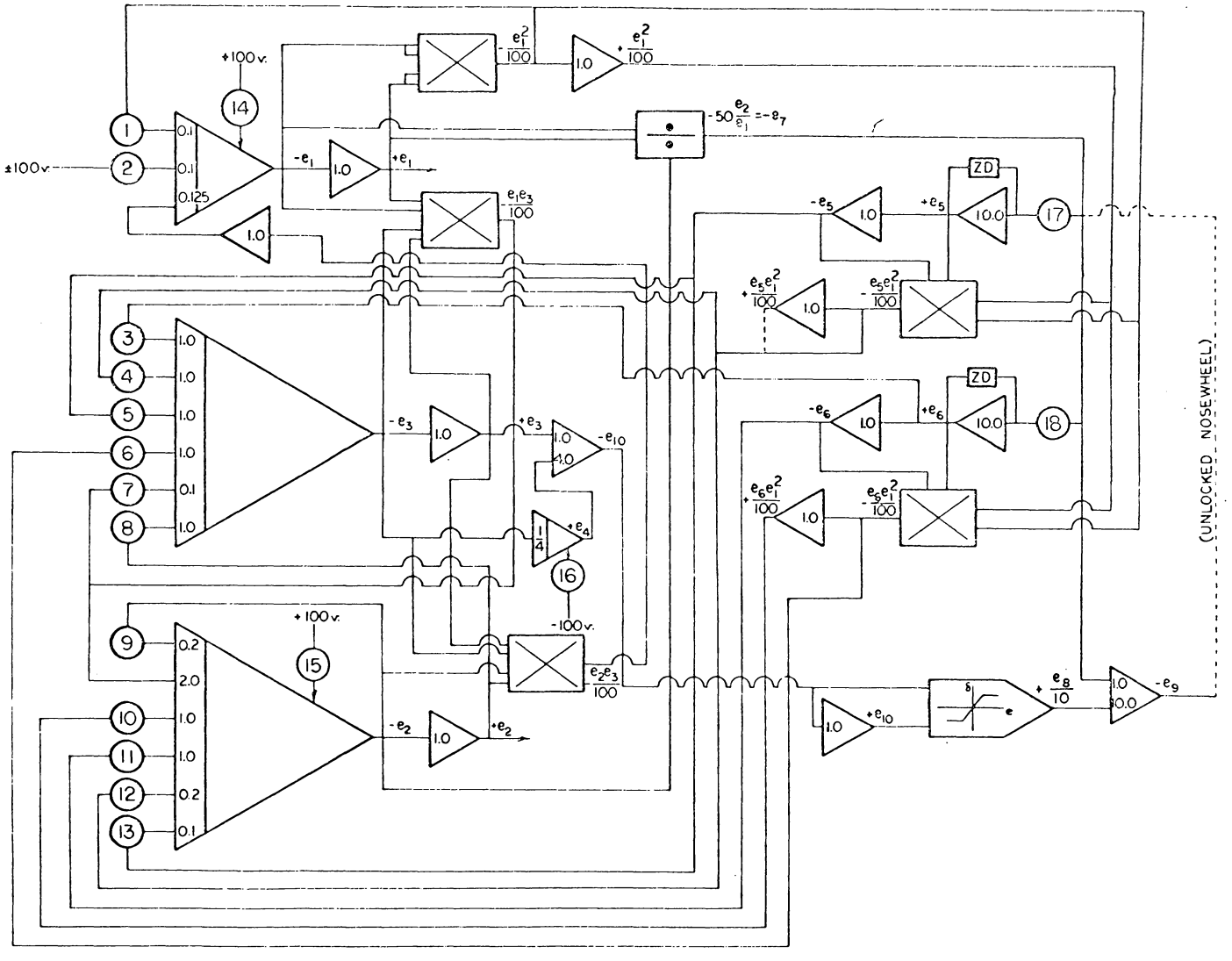

FIGURE C-2. COMPUTER SCHEMATIC

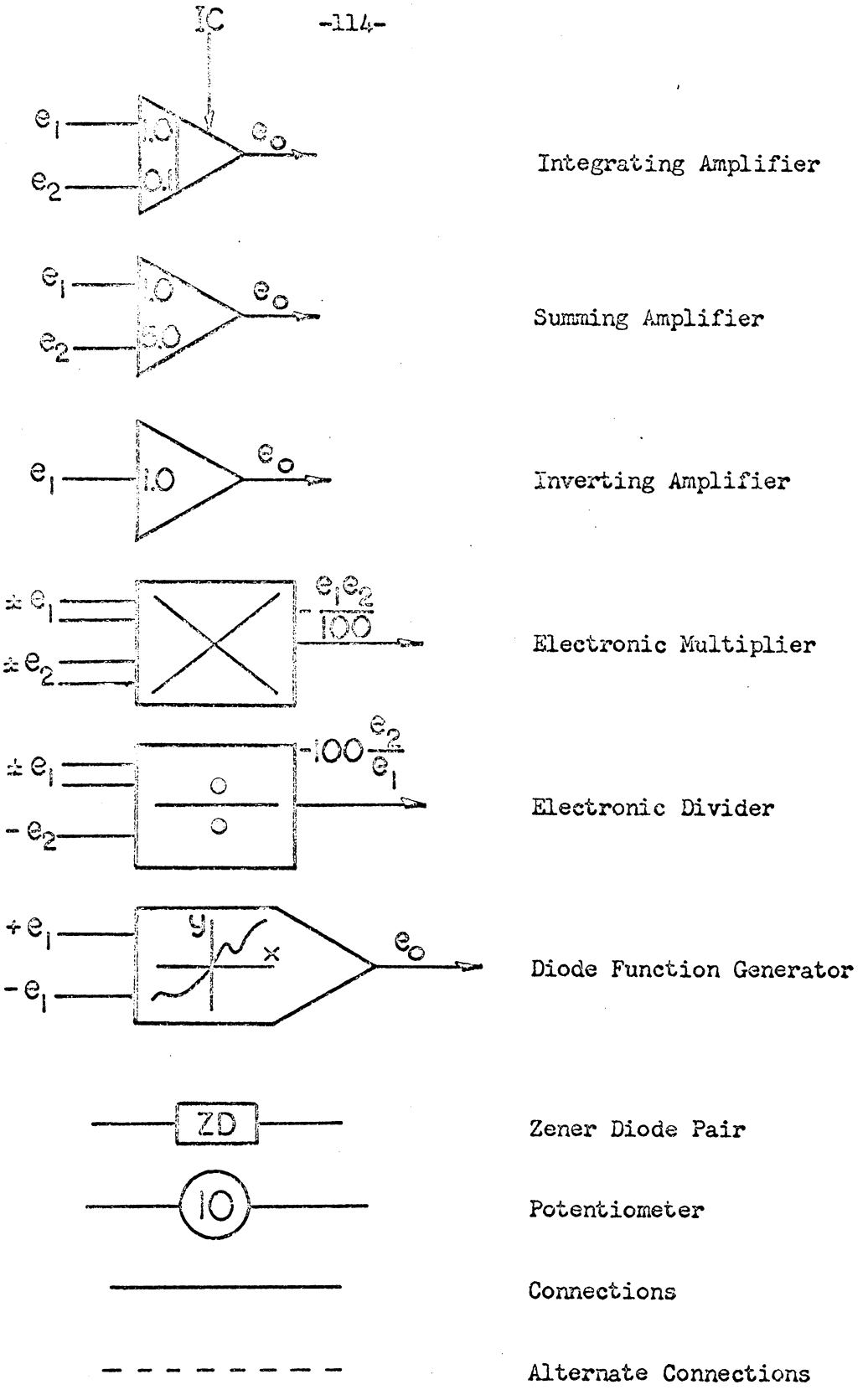
IC
e_1
e_2
1.0
0.1
e_o
Integrating Amplifier
e_1
e_2
1.0
3.0
e_o
Summing Amplifier
e_1
1.0
e_o
Inverting Amplifier
$\pm e_1$
$\pm e_2$
$-\frac{e_1 e_2}{100}$
Electronic Multiplier
$\pm e_1$
$-e_2$
$-100\frac{e_2}{e_1}$
Electronic Divider
$+e_1$
$-e_1$
y
x
e_o
Diode Function Generator
ZD
Zener Diode Pair
10
Potentiometer
Connections
Alternate Connections

Figure C-3

THE DIRECTIONAL STABILITY AND CONTROL OF AN AIRPLANE DURING THE LANDING ROLL

by

Andrew J. Gorechlad

ABSTRACT

This thesis considers the problem of the directional instability, as exhibited by aircraft with tricycle landing gear, during the landing roll after touchdown. The approximate equations of motion are solved on an analog computer to describe the motion of an aircraft as it moves along the runway after it has landed.

It is shown that during the landing roll the tricycle landing gear arrangement with a locked nosewheel is basically an unstable configuration. The principle cause of this instability is the nosewheel itself, since it contributes a large destabilizing component to the aircraft's overall directional stability. This undesirable influence can be reduced by using the elevator, or the horizontal tail, to keep the nosewheel lightly loaded during the landing roll.

Because of the inherent instability of a tricycle landing gear, some type of control is needed to keep the aircraft on the runway during the landing roll. Both the rudder and the nosewheel were

examined to determine their effectiveness as steering controls. It was found that the airplane is more easily controlled if either the elevator or the horizontal tail is used to reduce the load on the nosewheel.